HHS Public Access

Author manuscript

Toxicol Appl Pharmacol. Author manuscript; available in PMC 2020 December 24.

Published in final edited form as:

Toxicol Appl Pharmacol. 2020 December 15; 409: 115300. doi:10.1016/j.taap.2020.115300.

Biological effects of inhaled hydraulic fracturing sand dust VII. Neuroinflammation and altered synaptic protein expression

Krishnan Sriram[*], **Gary X. Lin**, **Amy M. Jefferson**, **Walter McKinney**, **Mark C. Jackson**, **Amy Cumpston**, **Jared L. Cumpston**, **James B. Cumpston**, **Howard D. Leonard**, **Michael Kashon**, **Jeffrey S. Fedan**

Health Effects Laboratory Division, National Institute for Occupational Safety and Health, Morgantown, WV 26505, United States of America

Abstract

Hydraulic fracturing (fracking) is a process used to recover oil and gas from shale rock formation during unconventional drilling. Pressurized liquids containing water and sand (proppant) are used to fracture the oil- and natural gas-laden rock. The transportation and handling of proppant at well sites generate dust aerosols; thus, there is concern of worker exposure to such fracking sand dusts (FSD) by inhalation. FSD are generally composed of respirable crystalline silica and other minerals native to the geological source of the proppant material. Field investigations by NIOSH suggest that the levels of respirable crystalline silica at well sites can exceed the permissible exposure limits. Thus, from an occupational safety perspective, it is important to evaluate the potential toxicological effects of FSD, including any neurological risks. Here, we report that acute inhalation exposure of rats to one FSD, *i.e.,* FSD 8, elicited neuroinflammation, altered the expression of blood brain barrier-related markers, and caused glial changes in the olfactory bulb, hippocampus and cerebellum. An intriguing observation was the persistent reduction of synaptophysin 1 and synaptotagmin 1 proteins in the cerebellum, indicative of synaptic disruption and/or injury. While our initial hazard identification studies suggest a likely neural risk, more research is necessary to determine if such molecular aberrations will progressively culminate in neuropathology/neurodegeneration leading to behavioral and/or functional deficits.

[*]Corresponding author at: Toxicology and Molecular Biology Branch, Health Effects Laboratory Division, National Institute for Occupational Safety and Health, 1000 Frederick Lane, Morgantown, WV 26508, United States of America. kos4@cdc.gov (K. Sriram).

CRediT authorship contribution statement

Krishnan Sriram: Conceptualization, Methodology, Investigation, Data curation, Writing (original draft), Writing (review & editing). **Gary X. Lin:** Methodology, Investigation. **Amy M. Jefferson:** Methodology, Investigation. **Walter McKinney:** Methodology, Software. **Mark C. Jackson:** Methodology, Software. **Amy Cumpston:** Investigation. **Jared L. Cumpston:** Investigation. **James B. Cumpston** Investigation. **Howard D. Leonard:** Investigation. **Jeffrey S. Fedan:** Conceptualization, Data curation, Writing (review & editing), Project administration, Funding acquisition.

5. Disclaimer

The findings and conclusions in this report are those of the authors and do not necessarily represent the official position of the National Institute for Occupational Safety and Health, Centers for Disease Control and Prevention. Mention of any company or product does not constitute endorsement by the National Institute for Occupational Safety and Health, Centers for Disease Control and Prevention.

Supplementary data to this article can be found online at https://doi.org/10.1016/j.taap.2020.115300.

Declaration of Competing Interest

The authors declare that they have no known competing financial interests or personal relationships that could have appeared to influence the work reported in this paper.

Keywords

Aluminum Silicates; Hydraulic Fracturing; Fracking Sand Dust; Neurotoxicity; Occupational Hazards; Silica

1. Introduction

Hydraulic fracturing (fracking) is a process used to recover oil and gas from shale rock formation during unconventional drilling. The technique involves fracturing the oil- and natural gas-laden rock with pressurized liquids. Water and sand make up 98 to 99.5% of the fluid used during fracking, and the rest includes chemical additives (Stringfellow et al. 2017). Sand is commonly used in the fracking fluid as a proppant to stabilize the fissures to facilitate oil and gas flow. Such fracturing is thought to allow for extended production yields from oil and gas wells, as well as extending the life of older/mature wells.

The transportation and handling of sand proppants at well sites can generate aerosols; thus, there is emerging concern of worker exposure to fracking sand dust (FSD) by inhalation. FSDs are generally composed of crystalline silica, besides other elements such as aluminum (Al), potassium (K), calcium (Ca), magnesium (Mg), manganese (Mn), iron (Fe) and cobalt (Co), depending on the geological source of the proppant material (Fedan et al. 2020). Field investigations conducted by the National Institute for Occupational Safety and Health (NIOSH) have shown that levels of respirable crystalline silica at well sites can exceed the established exposure limits for silica (Esswein et al. 2013). In some instances, the levels of respirable crystalline silica exceeded the occupational exposure limits by over 10-fold (Esswein et al. 2013). Thus, from an occupational safety perspective, it is of critical importance to evaluate the potential toxicological risks associated with FSD.

Ambient particulate matter from air pollution has been shown to cause nasal, olfactory and central neurotoxicity. Ultrastructural nasal pathology is seen in populations exposed to air pollutants (Calderon-Garciduenas et al. 2001). Neuroinflammation and oxidative stress in the nasal region of canines exposed to air pollution has been reported (Calderon-Garciduenas et al. 2003). Chronic brain inflammation, blood-brain barrier (BBB) disruption, and neuropathological changes were reported in humans exposed to fine and ultrafine particulate matter from air pollution (Calderon-Garciduenas et al. 2004, 2007). High levels of cyclooxygenase 2 (*Cox2/Ptgs2*) mRNA, an index of inflammation, was detected in the frontal cortex and hippocampal areas of autopsied brains from human subjects who had prolonged exposure to severe air pollution (Calderon-Garciduenas et al. 2004). There is also evidence to suggest that airborne solid ultrafine particles can deposit in the olfactory mucosa of the nasopharyngeal region of the respiratory tract and subsequently translocate *via* the olfactory nerve to deeper brain areas (Oberdörster et al. 2004).

In the drilling workplace environment, workers may be at risk for exposure to fine and/or ultrafine particulates largely *via* inhalation of such dusts. As FSD is composed predominantly of crystalline silica in the respirable range, the current studies were undertaken to examine the neural effects of FSD 8 (Fedan et al. 2020) inhalation in an experimental animal model. Principally, we evaluated changes in biogenic amine

neurotransmitters, neuronal synaptic protein expression, neuroinflammation and BBB-associated markers, as part of the initial hazard identification studies. Such efforts may aid in better understanding of the potential health effects of FSDs, if any, including the potential involvement of its constituent component/s. Besides, understanding the toxicological mechanisms can help improve and/or develop pre-job planning protocols, exposure assessment, exposure control and emergency preparedness programs to prevent adverse human health risks.

This is the seventh in a series of tandem papers describing investigations evaluating the potential toxicity of FSD 8 using a rat inhalation model. The approach to the overall investigation in the context of current knowledge about silica toxicity and research gaps was described in Fedan (2020). In the second paper (Fedan et al. 2020), FSD particle chemical and physical characteristics of nine FSDs collected at wells in the US in comparison to respirable crystalline silica (MIN-U-SIL® 5; MIN-U-SIL) and the effects of intratracheal (i.t.) instillation on the development of lung inflammation was investigated. One FSD (FSD 8) was used for toxicological investigation in organ systems, including lung, cardiovascular, immune and nervous systems (Russ et al. 2020; Anderson et al. 2020; Sager et al. 2020; Krajnak et al., 2020; present study), as well as cytotoxicity (Olgun et al. 2020), and the collective results have been summarized (Investigative Team 2020).

2. Methods

2.1. Animals

All studies were conducted in facilities accredited by AAALAC International, were approved by the Institutional Animal Care and Use Committee and were in compliance with the Public Health Service Policy on Humane Care and Use of Laboratory Animals and the NIH Guide for the Care and Use of Laboratory Animals. Male Sprague-Dawley rats ([H1a: (SD) CVF, approximate body weight of 200–275 g at arrival, were obtained from Hilltop Lab Animals, Inc. (Scottdale, PA). All animals were free of viral pathogens, parasites, mycoplasm, *Helicobacter* and cilia-associated respiratory bacillus. Animals were acclimated for 1 wk., housed in pairs in ventilated micro-isolator units supplied with HEPA-filtered laminar flow air (Thoren Caging Systems; Hazleton, PA), with 7090 Sani Chip and 7070C Diamond Dry combination (both from Harlan, now Envigo; Indianapolis, IN) for bedding, and provided tap water and 2918 irradiated Teklad Global 18% rodent diet (Harlan, now Envigo; Indianapolis, IN) *ad libitum.* Rats were housed under controlled light cycle (12 h light/12 h dark) and temperature (22–25 °C) conditions.

2.2. Whole-body inhalation exposure to FSD 8

The FSD used in this study was FSD 8, collected from a well pad in the U.S. during fracking operations. A summary of the physicochemical characteristics and elemental composition of FSD 8 and eight other FSDs, as well as MIN-U-SIL, is provided in Fedan et al. (2020) and Russ et al. (2020).

An acoustical particle generator system (McKinney et al. 2013) with modifications (Russ et al. 2020) was used to generate FSD 8 aerosols. Rats were independently exposed to two

concentrations of FSD 8 (10 or 30 mg/m^3, low and high dose, respectively) for 6 h/d for 4 consecutive days. Concurrently, another set of rats that served as controls were exposed to HEPA-filtered air in an identical exposure system. The exposures were conducted in two experimental blocks to obtain a final $n = 8$ for each experimental group. During the daily 6-h whole-body inhalation exposures, the animals did not have access to food or water. Animals exposed under such conditions did not exhibit any observable pain or distress, body weight changes, behavioral abnormalities or adverse health effects.

2.3. Euthanasia and sample collection

In both the low and high dose FSD 8 studies, animals were euthanized at 1, 7 or 27 d after cessation of exposure. Additionally, in the high dose FSD 8 study, one set of animals were euthanized 90 d after cessation of exposure to determine long-term neural effects, if any. On any given day, a total of 8 animals (four air-exposed and four FSD 8 exposed animals per time point) were designated for brain microdissections. Euthanasia was performed by administration of an intraperitoneal injection of sodium pentobarbital (Fatal Plus; 100–300 mg/kg; Vortech Pharmaceutical Ltd., Dearborn, MI), and the animals were exsanguinated by transecting the abdominal aorta. Death was confirmed by lack of pedal reflex (response to firm toe pinch). After euthanasia and collection of lung lavage fluid for pulmonary toxicity assessment, the brains were excised and discrete brain areas, olfactory bulb (OB), hippocampus (HIP), striatum (STR) and cerebellum (CER) from the left and right hemispheres were dissected. All brain tissue sampling was completed before 11:00 am to negate any potential influence of circulating corticosterone on neural markers, and thereby, the experimental outcome. Following euthanasia, excision of the whole brain and microdissections of both hemispheres was accomplished within 4–5 min. Microdissections were performed on a thermoelectric cold plate (Model TCP-2, Thermoelectrics Unlimited, Inc., Wilmington, DE). As and when brain regions were dissected out, the tissues were immediately transferred to the tubes containing the appropriate storage reagent and frozen at −75 °C until use.

Tissues from the left hemisphere were collected in 1% perchloric acid and stored at −75 °C until processing for biogenic amine neurotransmitter analysis. Tissues from right hemisphere were collected in Tissue Protein Extraction Reagent (T-PER, Pierce Biotechnologies, Inc.; Rockford, IL) containing protease inhibitor cocktail and EDTA, and were stored at −75 °C until processing for the isolation of RNA and proteins for real-time PCR or immunoblot analysis, respectively.

2.4. High performance liquid chromatography with electrochemical detection (HPLC-EC)

Biogenic amines, norepinephrine (NE), epinephrine (EPI), dopamine (DA), and serotonin (5-hydroxytryptamine, 5-HT), as well as some of their metabolites, *e.g.,* dihydroxyphenyl acetic acid, (DOPAC), homovanillic acid (HVA) and 5-hydroxyindole acetic acid (5-HIAA), were measured by HPLC-EC (Sriram et al. 2014). Briefly, brain tissues were homogenized in 1% perchloric acid containing isoproterenol (as internal standard) and centrifuged for 10 min at 12,000 × *g*. The supernatant was filtered through a 0.2 μ nylon filter and 10 μl aliquots were injected onto a C-18 reverse phase HPLC column (Agilent Technologies; Santa Clara, CA) using an UltraFast Liquid Chromatography (UFLC) system (Shimadzu

Instruments; Columbia, MD) attached to an autosampler. A BASLC4B amperometric detector (BASi Inc.; West Lafayette, IN) with a glassy carbon oxidative flow cell was used for detection at an electrode potential of 0.8 V. The mobile phase (pH 3.2) consisted of 0.15 M monochloroacetic acid, 0.115 M sodium hydroxide, 0.1 mM EDTA, 0.015% sodium octyl sulfate, 3% acetonitrile, 1.5% methanol and 1.2% tetrahydrofuran. Under these conditions NE, EPI, DA, 5-HT, DOPAC, HVA and 5-HIAA were chromatographically separated and detected. Analytes were quantified by comparing peak area detector responses in the sample with those produced by a series of standards similarly prepared in 1% perchloric acid. The pellet from each of the processed sample was solubilized with 3% sodium hydroxide and the protein content was estimated. The neurotransmitter content in each sample was then normalized to the amount of protein. The values were calculated as ng/mg total protein and are graphically represented as percent of air-exposed controls.

2.5. Preparation of brain tissues for protein and RNA isolation

Selected brain tissues were homogenized in 0.3 ml of T-PER tissue protein extraction reagent (Pierce Biotechnologies, Inc.) containing protease inhibitors and EDTA. Aliquots of the homogenate (0.15 ml) were collected into separate 1.5-ml microfuge tubes and centrifuged at 9600 ×*g* for 5 min to pellet the cell/tissue debris. The supernatants were carefully recovered, without disturbing the pellet and transferred to new 1.5-ml centrifuge tubes. The supernatants were stored at −20 °C until protein concentrations were determined.

To the remaining homogenate, 0.7 ml of TRI Reagent® (Molecular Research Center, Inc.; Cincinnati, OH) and 0.2 ml of chloroform were added. The homogenates were stored at −20 °C until RNA isolation.

2.6. Protein estimation

On the day of protein estimation (usually the following day after supernatants were prepared), the samples were thawed on ice and vortexed. Total protein in the supernatant was determined according to the micro-bicinchoninic acid method (Pierce Biotechnologies, Inc.) using bovine serum albumin as a standard. For long-term storage, the protein extracts were kept at −75 °C.

2.7. RNA isolation, cDNA synthesis and real-time PCR

On the day of RNA isolation, the homogenates that were processed and stored for RNA isolation were thawed at room temperature, vortexed and transferred to MaXtract High Density gel (Qiagen; Valencia, CA) tubes. The tubes were centrifuged at 9600 ×*g* for 2 min to separate the organic and aqueous phase. The aqueous phase (0.45 ml) was collected into fresh 1.5-ml microfuge tubes and 0.24 ml of 200-proof ethanol was added drop-wise while gently vortexing. The entire mixture was then transferred to RNeasy mini spin columns (Qiagen) for RNA isolation as suggested by the manufacturer. After elution of the RNA with water, the concentrations were determined using the NanoDrop® ND-1000 UV–Vis spectrophotometer (NanoDrop Technologies; Wilmington, DE). The isolated RNA was then stored at −75 °C until use.

First strand cDNA synthesis was carried out using total RNA (1 μg), random hexamers and MultiScribe™ reverse transcriptase (High Capacity cDNA Reverse Transcription Kit; Applied Biosystems; Foster City, CA) in a 20 μl reaction. Reverse transcription reactions were scaled up to obtain larger amounts of cDNA as necessary. Real-time PCR amplification was performed using the 7500 Real-Time PCR System (Applied Biosystems) in combination with TaqMan® chemistry. Specific primers and FAM™ dye-labeled TaqMan® MGB probe sets (TaqMan® Gene Expression Assays) were procured from Applied Biosystems and used according to the manufacturer's recommendations. In some experiments, focused low-density gene signature arrays (384-well microfluidic card; TaqMan® rat inflammation panel) was used to identify potential inflammatory pathways. Specifically, the mRNA expression of genes associated with the arachidonic acid pathway (*Alxo5, Ltc4s, Pla2g2d, Ptgs1 and Ptgs2*) were obtained from the rat inflammation gene signature array. For genes that exhibited very low expression in certain brain areas, a pre-amplification (14 cycles) was performed prior to routine PCR analysis. All PCR amplifications (45 cycles) were performed in a total volume of 25 μl, containing 5 μl of diluted cDNA, 1.25 μl of the specific TaqMan® Gene Expression Assay and 12.5 μl of TaqMan® Gene Expression Master mix (Applied Biosystems), respectively. Sequence detection software (version 1.7; Applied Biosystems) results were exported as tab-delimited text files and imported into a spread sheet for further analysis. Following normalization to *Actb* mRNA, relative quantification of gene expression was performed using the comparative threshold (C_T) method as described by the manufacturer (Applied Biosystems; User Bulletin 2). There were no differences in the basal mRNA expression (control) levels within a region or time point among the different exposure regimens. However, mRNA expression levels varied between regions, and this is to be expected given the cellular heterogeneity of various brain areas. Fold change values were calculated and are graphically represented as percent of air-exposed controls to depict increase or decrease in mRNA expression.

2.8. Western immunoblotting

Aliquots of brain homogenates (6 μg total protein) diluted 1:1 in 2× Laemmli sample buffer were boiled and loaded onto 10% SDS-polyacrylamide gels. Proteins then were electrophoretically resolved and transferred to 0.45 μm Immobilon-FL PVDF Membranes (Millipore, Billerica, MA). Following transfer, immunoblot analysis was performed. Briefly, membranes were blocked using Odyssey Blocking Buffer (LI-COR Biosciences, Lincoln, NE) for 1 h at room temperature, washed (1 × 5 min; 2 × 10 min) with phosphate-buffered saline containing Triton X-100 (PBST), and incubated overnight at 4 °C with the primary antibodies (30–50 ng/ml primary antibody buffer) to synaptophysin 1 (SYP; cat# sc-17750, mouse monoclonal, Santa Cruz Biotechnology, Inc.; Santa Cruz, CA; 35 kDa), synaptotagmin 1 (SYT; cat# sc-136480, mouse monoclonal, Santa Cruz Biotechnology, Inc.; 60 kDa), tyrosine 3-monooxygenase/tryptophan 5-monooxygenase activation protein-ε (YWHAE or 14–3-3ε; cat# sc-23957, mouse monoclonal, Santa Cruz Biotechnology, Inc.; 28 kDa), glial fibrillary acidic protein (GFAP; cat# Z0334, rabbit polyclonal, DAKO North America Inc., Carpinteria, CA; 50 kDa) or myelin basic protein (MBP; cat# sc-13914, goat polyclonal, Santa Cruz Biotechnology, Inc.; recognizes various isoforms ranging from 14 to 21.5 kDa; the expression of the predominant 18.5 kDa isoform was assessed in this study).

β-actin (ACTB; cat# sc-47778, mouse monoclonal, Santa Cruz Biotechnology, Inc.; 46 kDa) was used as an endogenous control. Following incubation with appropriate primary antibodies, blots were washed with PBST (1 × 5 min; 3 × 10 min) and incubated for 1 h at room temperature with appropriate IRDye 680 or 800 Secondary Antibodies (LI-COR Biosciences, Lincoln, NE). The membranes were protected from light to minimize any photo-bleaching of the fluorescent dyes. Membranes were washed (1 × 5 min; 4 × 10 min) in PBST, followed by washes (2 × 3 min) in PBS. Near-infrared fluorescence detection was performed using the Odyssey Imaging System (LI-COR Biosciences). The fluorescent signal intensities (k counts) of the individual bands were determined and normalized to ACTB. There were no differences in the basal mRNA expression (control) levels within a region or time point among the different exposure regimens. However, protein expression levels varied between regions, and this is to be expected given the cellular heterogeneity of various brain areas. The data are graphically represented as percent of air-exposed controls to depict increase or decrease in protein expression.

2.9. Statistical analysis

The exposures of rats to low and high FSD 8 particulate exposures were run separately. Each exposure had a control (filtered Air) group associated with it and was utilized to calculate percent change from the control group for each variable. For statistical analysis, the control groups from the two exposure runs were combined into a single, 0-dose control group. The statistical analysis incorporated both dose and days post- exposure by running two-way ANOVAs for each independent variable. Some variables were transformed using the natural log upon evidence of heterogeneity of variance and reanalyzed. Post-hoc comparisons between treatment groups at each time were generated using Fishers LSD test. The data analysis reported in this paper was generated using SAS/STAT software Version 9 for the SAS System for Windows. Exploratory data analysis was performed using JMP software Version 13. Outliers were identified using the 'Robust Fit Outliers' function in JMP. Outliers were detected in the mRNA data files and 7 values from 5 different animals were eliminated from a total of 2160 measures across 5 genes.

The results are presented as means ± SE. Results were considered significant at $P < 0.05$, and more stringent significance levels have been labeled in the figures, *viz.*, $^{*}P < 0.05$, $^{**}P < 0.01$, $^{***}P < 0.001$ are indicative of significance from the corresponding air-exposed control. $^{\#}$, $^{\#\#}$ or $^{\#\#\#}$ indicates values significantly different from high dose FSD 8 at $P < 0.05$, 0.01 or 0.001, respectively. $^{+}$, $^{++}$ or $^{+++}$ indicates values significantly different from low dose FSD 8 at $P < 0.05$, 0.01 or 0.001, respectively.

3. Results

3.1. FSD 8 elicits brain-region specific neuroinflammation

Neuroinflammation has been linked to the pathogenesis of various neurotoxic and neurodegenerative disease conditions (Mogi et al. 1994; Hunot et al. 2001; McGeer and McGeer 2004; Sriram et al. 2002, 2006a, 2006b). Neuroinflammation can contribute to neurotoxicity following exposure to metal particulate aerosols (Sriram et al. 2010a, 2010b). We, therefore, analyzed neuroinflammatory responses in the brain using low-density

inflammatory gene PCR arrays (TaqMan® gene signature array) or specific assays for proinflammatory mediators. The relative mRNA expression was assessed by TaqMan® real-time polymerase chain reaction (PCR) analysis.

Exposure to the low dose of FSD 8 caused up-regulation of *Alox5* mRNA in the OB (Fig. 1) at 1 d (53%) and 7 d (24%) post-exposure. The expression of *Ltc4s* mRNA in OB also increased (44%) at 1 d after the low dose FSD 8 exposure. In the OB, increased expression of *Pla2g2d* mRNA was seen at all the time points examined. *Pla2g2d* mRNA expression in the OB was upregulated by 38%, 33% and 59% respectively, at 1, 7 and 27 d post-exposure. A transient increase (33%) of *Ptgs2* mRNA was observed in the OB at 7 d post-exposure. In the HIP (Fig. 2), the low dose FSD 8 caused a transient up-regulation of *Alox5* mRNA at 7 d (67%) post-exposure. The expression of *Ltc4s* mRNA in the HIP was not affected by the low dose FSD 8 exposure. Large increases in the expression of *Pla2g2d* mRNA was detected in the HIP at all the time points examined. *Pla2g2d* mRNA expression in the HIP was upregulated by 118%, 110% and 188%, respectively, at 1, 7 and 27 d post-exposure. Similarly, large increases in *Ptgs1* mRNA was seen in the HIP at 1 d (142%) and 7 d (213%) post-exposure, respectively. High levels of *Ptgs2* mRNA were also seen in the HIP at 7 d (158%) and 27 d (135%) post-exposure, respectively. In the CER (Fig. 3), the low dose of FSD 8 caused a transient up-regulation of *Alox5* mRNA at 1 d (50%) post-exposure, and, by 27 d, the expression was down-regulated (36% decrease). The expression of *Ltc4s* mRNA in the CER remained unaffected at the earlier time points but was down-regulated at 27 d after the low dose FSD 8 exposure (55% decrease). Early increases in the expression of *Pla2g2d* (51%), *Ptgs1* (81%) and *Ptgs2* (86%) mRNAs was seen in the CER at 1 d post-exposure, followed by down-regulation of these genes by 27 d post-exposure (43–61% decrease).

Exposure to the high dose FSD 8 (30 mg/m^3), caused up-regulation of *Alox5* mRNA in the OB (Fig. 1) at all the time points examined. *Alox5* mRNA expression in the OB was upregulated by 43%, 74% and 36%, respectively, at 1, 7 and 27 d post-exposure. A transient increase in *Ltc4s* mRNA in the OB (36%) was seen 7 d after the high dose FSD 8 exposure. Likewise, a transient up-regulation in the expression of *Pla2g2d* mRNA (44%) and *Ptgs1* mRNA (69%) occurred in the OB at 1 d and 7 d post-exposure, respectively. Early increases in *Ptgs2* mRNA was seen in the OB at 1 d (35%) and 7 d (74%) following exposure to a high dose of FSD 8. In the HIP (Fig. 2), the high dose FSD 8 mostly resulted in down-regulation of genes associated with arachidonic acid pathway. The expression of *Alox5* mRNA in the HIP was transiently down-regulated at 7 d (70% decrease) post-exposure. The expression of *Ltc4s* mRNA in the HIP was also transiently down-regulated at 7 d (67% decrease) post-exposure. A small increase in the expression of *Pla2g2d* mRNA was seen in the HIP at 1 d (23%) that was followed by down-regulation of its expression (82% decrease) 7 d post exposure. Increased expression of *Ptgs1* mRNA in the HIP occurred at 7 d (136%) after the high-dose FSD 8 exposure. The expression of *Ptgs2* mRNA in the HIP was also transiently down-regulated at 7 d (55% decrease) post-exposure. In the CER (Fig. 3), the high dose FSD 8 did not significantly alter the expression of the arachidonic acid pathway genes. Only a transient down-regulation of *Ptgs1* mRNA at 1 d (31% decrease) and of *Pla2g2d* (55% decrease) at 27 d post-exposure was observed.

While the expression of the genes associated with the arachidonic acid pathway occurred early, the expression of interleukin 6 (*Il6*) and the inducible form of nitric oxide synthase (*Nos2*; iNos), in general, exhibited a delayed response in all the brain areas examined. Exposure to the low dose FSD 8 caused significant increases in the mRNA expression of *Nos2* and/or *Il6* in the OB (Fig. 4), HIP (Fig. 5) and CER (Fig. 6) at 27 d, but not at earlier time points. Up-regulation of *Nos2* mRNA was seen in OB (122.6%) and HIP (173%), 27 d after low dose FSD 8 exposure. Similarly, up-regulation of *Il6* mRNA was seen in OB (60%), HIP (103%) and CER (71%), 27 d after low dose FSD 8 exposure. In the CER of low dose FSD 8-exposed animals, a transient down-regulation of *Il6* mRNA was observed, 1 d after exposure (49.7% decrease).

Exposure to the high dose FSD 8, in general, did not elicit an inflammatory response in all the brain areas examined. A small up-regulation in *Il6* mRNA resulted only in the OB (Fig. 4) at 7 d (37.5%) and 27 d (53.6%) post-exposure. A transient down-regulation of *Nos2* (55.3% decrease) and *Il6* (55.7% decrease) mRNAs was seen in the HIP (Fig. 5), 7 d after exposure to the high dose FSD 8. In the CER (Fig. 6), a transient down-regulation of *Nos2* (40.5% decrease) and *Il6* (41.1% decrease) mRNAs occurred 1 d after exposure to the high dose FSD 8.

3.2. FSD 8 alters the expression of blood-brain barrier associated markers

Systemic inflammatory and oxidative stress events have been shown to disrupt the BBB (Huber et al. 2001; Thiel and Audus 2001). As neuronal injury is often associated with cerebrovascular dysfunction and modification of BBB function, we examined whether exposure to FSD 8 affected the integrity of the BBB. For this, we analyzed the expression of specific markers of blood-brain barrier endothelium, like the tight junction proteins, claudin 1 (*Cldn1*) and claudin 3 (*Cldn3*). In addition, we also examined the expression of matrix metalloproteinase 9 (*Mmp9*), a pro-inflammatory protease that is upregulated and released by glial cells like microglia and oligodendroglia, following stimulation by inflammatory cytokines. The relative mRNA expression was assessed by TaqMan® real-time polymerase chain reaction (PCR) analysis.

Exposure to the low dose of FSD 8 did not alter the expression of *Mmp9* or *Cldn3* mRNAs in the OB (Fig. 7) but caused a transient up-regulation of *Cldn1* mRNA (71%) in this region at 7 d post-exposure. In the HIP (Fig. 8), the low dose of FSD 8 caused up-regulation of *Mmp9* (75%) and *Cldn1* (63%) mRNAs, 27 d post-exposure. *Cldn3* mRNA was down-regulated in the HIP at 7 d (81.3% decrease) and 27 d (78.9% decrease) post-exposure. In the CER (Fig. 9), the low dose of FSD 8 did not affect Mmp9 mRNA expression but caused down-regulation of *Cldn1* mRNA at 1 d (41.4% decrease) and 7 d (38.2% decrease) after cessation of exposure. *Cldn3* mRNA was transiently up-regulated in the CER at 1 d (77%) post-exposure.

Exposure to the high dose FSD 8 caused up-regulation (59%) of *Mmp9* mRNA in the OB (Fig. 7), 7 d after last FSD 8 exposure. The high dose FSD 8 also caused a transient up-regulation of *Cldn3* mRNA in the OB (52.4%), 1 d after exposure. The expression of *Mmp9, Cldn1* and *Cldn3* were unaltered in the HIP (Fig. 8) following the high dose FSD 8 exposure. In the CER (Fig. 9), *Cldn1* mRNA was down-regulated (42% decrease) 1 d after

FSD 8 exposure and *Mmp9* mRNA was down-regulated (39% decrease) 7 d after FSD 8 exposure.

3.3. FSD 8 causes brain-region specific changes in biogenic amine neurotransmitters

Neurotransmitters play a critical role in neuronal communication and maintenance of brain function. Abnormality or dysregulation of the physiological levels of neurotransmitters can potentially result in neuronal dysfunction and pathogenesis. Metal aerosols and particulate matter have been shown to interact with and/or affect various neurotransmitter systems, such as adrenergic, dopaminergic, serotonergic, cholinergic and GABAergic pathways (Tin-Tin-Win-Shwe et al., 2008; Allen et al. 2014; Sriram et al. 2014). We, therefore, investigated whether exposure to FSD 8 aerosol would likewise affect NE, EPI, DA and 5-HT contents in the brain using HPLC-EC.

In rats exposed to a low dose of FSD 8, a small but significant increase in NE (13%) occurred in the HIP (Fig. 10), 7 d after exposure. Similarly, a significant increase in NE (44%) resulted in STR (Fig. 10) at 7 d. NE levels returned to baseline (control) values by 27 d in these regions. NE remained unchanged in the OB and CER (Fig. 10) at all the time points examined, after the low dose of FSD 8 exposure. A high dose of FSD 8 did not alter NE levels in any of the brain areas evaluated (Fig. 10).

A significant increase in EPI (29%) was observed in the HIP (Fig. 11) 7 d after exposure to a low dose of FSD 8, which returned to control values by 27 d. In the STR (Fig. 11), a reduction in EPI (25% decrease) was seen at 1 d. The levels increased (32%) by 7 d before returning to control values by 27 d. EPI levels remained unchanged in the OB and CER (Fig. 11) at all the time points examined, after the low dose FSD 8 exposure. A high dose of FSD 8 caused a significant increase in EPI levels (38%) in the OB (Fig. 11) at 7 d, which returned to control values by 27 d. The high dose of FSD 8 also caused significant reductions of EPI in the STR (26% decrease; Fig. 11) and CER (29% decrease; Fig. 11) at 7 d. EPI levels in these regions returned to control values by 27 d (Fig. 11).

The low dose of FSD 8 also caused a significant increase in DA levels in the HIP (44%; Fig. 12) and STR (22%; Fig. 12) at 7 d post-exposure, which returned closer to control values by 27 d. The levels of the DA metabolites, DOPAC and HVA, were also altered following exposure to the low dose of FSD 8. HVA levels, but not DOPAC, increased in the HIP (37%; Table 1) at 7 d and recovered to control values by 27 d. On the other hand, DOPAC levels, but not HVA levels, decreased in the STR (22% decrease; Table 2) at 27 d. The metabolite ratios were unaltered in the HIP and STR (Tables 3 and 4). In the CER (Fig. 12), a small but significant increase in DA (18%) was seen at 1 d that returned to control values by 7 d. The metabolites or metabolite ratios of were unaltered in the CER (Tables 4 and 6). DA levels did not change in the OB (Fig. 12) after a low dose FSD 8 exposure, but a small decrease in DOPAC/DA ratio (16% decrease; Table 3) was observed in this region. However, the high dose of FSD 8 caused a small but significant reduction of DA in the OB (22% decrease; Fig. 12) at 7 d that returned to control values by 27 d. Both DOPAC and HVA were reduced in the OB (22% and 21% decrease respectively; Table 3) 7 d after high dose FSD 8 exposure and recovered to control values by 27 d. The metabolite ratios remained unaffected in the

CER after a high dose FSD 8 exposure (Table 4). DA levels were unaltered in the HIP, STR and CER after a high dose of FSD 8 (Fig. 12).

In rats exposed to the low dose of FSD 8, a significant reduction in the levels of 5-HT (33% decrease) was seen in the OB (Fig. 13) at 27 d post-exposure. On the other hand, small increases in 5-HT resulted in the HIP (15%; Fig. 13) at 7d, STR (17–19%; Fig. 13) at 1 and 7 d, and CER (28%; Fig. 13) at 1 d. 5-HT levels were similar to control values in the HIP, STR and CER after 27 d. The high dose of FSD 8 also caused a small but significant reduction of 5-HT in the HIP (19% decrease; Fig. 13) at 27 d. 5-HT levels were unaltered in the OB, STR and CER after a high dose of FSD 8 (Fig. 13). The levels of 5-HIAA, the metabolite of 5-HT, remained unaffected in all brain areas examined (Tables 1 and 2); however, a significant increase in the 5-HIAA/5-HT metabolite ratio (38%; Table 5) occurred in the OB, 27 d after the low dose FSD 8 exposure. The metabolite ratios remained unaffected in other brain regions (Tables 5–6).

3.4. FSD 8 causes brain-region specific changes in the expression of neuronal synaptic proteins

Since FSD 8 altered biogenic amine neurotransmitters in various brain regions, we examined whether FSD 8 also affected neuronal synaptic proteins, given their involvement in transport and release of neurotransmitters. Specifically, we evaluated changes in the synaptophysin (SYP), a major integral membrane protein of synaptic vesicles and a key presynaptic marker, synaptotagmin 1 (SYT1), a critical calcium sensor associated with neurotransmitter release, and YWHAE (14–3-3-ε), a synaptic membrane protein that is involved in regulating short- and long-term synaptic plasticity. The expression levels of these proteins were determined by western immunoblot analysis.

Exposure to the low dose of FSD 8 aerosol did not affect SYP protein content in the OB (Fig. 14 and S1A). However, significant reductions in SYP protein was seen in HIP (36% decrease; Fig. 14 and S1B) at 27 d post-exposure and in the STR (23% decrease; Fig. 14 and S1C) at 1 d after cessation of exposure. In the CER (Fig. 14 and S1D), a large increase in SYP protein (88%) was observed at 27 d after exposure to the low dose of FSD 8. The high dose of FSD 8 caused a time-dependent increase in SYP protein (36%, 53% and 131%) in the OB at 1, 7 and 27 d post-exposure periods, respectively (Fig. 14 and S1A). The SYP protein levels recovered to baseline (control) levels by 90 d. In the STR (Fig. 14 and S1C), the high dose of FSD 8 caused a transient reduction (31.6% decrease) at 1 d that recovered to control levels by 7 d and remained unaltered until 90 d. In the CER (Fig. 14 and S1D) of the high dose FSD 8 exposed animals, SYP protein levels remained persistently lower (42.2%, 33.1% and 39.9% decrease) at 7, 27 and 90 d, respectively.

Following exposure to the low dose of FSD 8, an early increase in SYT protein (24%) was seen in the OB (Fig. 15 and S2A) at 1d post-exposure, but by 7 d the levels were below control (18.4% decrease). SYT protein content in the HIP (Fig. 15 and S2B) was not affected by the low dose FSD 8 exposure. In the STR (Fig. 15 and S2C), a small reduction (18.7% decrease) was seen at 1 d but remained unaffected at other time points examined. In the CER (Fig. 15 and S2D), an increase in SYT protein (35.1% decrease) occurred at 1 d, but the levels were reduced (14% decrease) to below control values by 27 d after low dose

FSD 8 exposure. The high dose of FSD 8 caused a transient increase in SYT protein (21.7%) in the OB (Fig. 15 and S2A) at 1 d, but the levels were reduced to below control values (18.7% decrease) at 27 d post-exposure. In the HIP (Fig. 15 and S2D), the high dose FSD 8 caused a transient reduction of SYT (31.1% decrease) at 1 d that rebounded to cause an increased expression by 27 d (27.9%) before returning to control levels by 90 d. A small but significant increase (20.1%) was seen in the STR (Fig. 15 and S2C) at 27 d, but not at other time points examined. In the CER (Fig. 15 and S2D) of the high dose exposed animals, SYT protein levels transiently increased (25.8%) at 1 d post-exposure, followed by a persistent reduction (27.5%, 25.8% and 24.6% decrease) at 7, 27 and 90 d, respectively.

Following exposure to the low dose of FSD 8, an early increase in YWHAE protein (112.1%) occurred in the OB (Fig. 16 and S3A) at 1 d post-exposure, but by 7 d the levels returned to control values. YWHAE protein content in the HIP (Fig. 16 and S3B) was also reduced (21.1% decrease) at 1 and 7 d following the low dose FSD 8 exposure. YWHAE protein in the STR (Fig. 16 and S3C) was not affected by the low dose FSD 8 exposure. In the CER (Fig. 16 and S3D), the low dose of FSD 8 caused a large increase (54.7%) by 7 d but remained unaffected at other time points examined. The high dose of FSD 8 caused a transient increase in YWHAE protein (44.8%) in the OB (Fig. 16 and S3A) at 7 d but the levels recovered to control values by 27 d and remained unaltered at 90 d. In the HIP (Fig. 16 and S3B), the high dose FSD 8 caused elevated YWHAE levels at 27 d (17.2%) and 90 d (34.6%), respectively. A small but significant increase in YWHAE (18.1%) was seen in the STR (Fig. 16 and S3C) at 1 d that was followed by a large reduction (50.9% decrease) by 7 d, after which the levels recovered to control values and remained unaltered by 90 d. In the CER (Fig. 16 and S3D) of the high dose exposed animals, YWHAE protein levels were persistently lower (18.5%, 23% and 30.6% decrease) at 7, 27 and 90 d, respectively, consistent with the changes seen with SYP and SYT expression in this region.

3.5. FSD 8 causes astroglial activation

Glial cells are involved in the immune response of the brain and are activated by subtle changes in neuronal milieu following neuronal perturbation or injury (Kreutzberg 1996; Streit, 1999). Astrocytes, in particular, are recognized to undergo hypertrophy in response to local neural damage. The hallmark of this response is enhanced expression of the intermediate filament protein, glial fibrillary acidic protein (GFAP). Besides, astrocytes are key regulators of synapse formation and synaptic transmission (Allen, 2014; Farhy-Tselnicker and Allen, 2018). Thus, assessment of astroglial activation can serve as an index of an underlying synaptic and/or neuronal perturbation or injury. Expression of GFAP was assessed by western immunoblot analysis.

Exposure to the low dose FSD 8 aerosol did not affect GFAP protein content in the OB (Fig. 17 and S4A) or CER (Fig. 17 and S4D). A small and delayed up-regulation of GFAP protein (21%) was seen in the HIP (Fig. 17 and S4B) at 27 d post-exposure. In the STR (Fig. 17 and S4C), a small but significant reduction in GFAP protein (33% decrease) was observed 7 d after the last FSD 8 exposure.

The high dose of FSD 8 induced GFAP protein expression in all the four brain regions (OB, HIP, STR, CER) examined. In the OB (Fig. 17 and S4A), the high dose FSD 8 caused a

robust increase in GFAP protein content (200%) by 1 d, which recovered to control values by 7 d and remained unchanged thereafter. In the HIP (Fig. 17 and S4B), the high dose FSD 8 caused a small increase in GFAP protein content (26.8%) by 27 d, which recovered to control values by 90 d. In the STR (Fig. 17 and S4C), the high dose FSD 8 caused an increase in GFAP protein content (53%) by 7 d that remained elevated at 27 d before returning to control values by 90 d. In the CER (Fig. 17 and S4D), the high dose FSD 8 caused a large increase in GFAP protein content (91.6%) by 7 d that recovered to control values by 27 d and remained unchanged at 90 d.

3.6. FSD 8 alters the expression of the oligodendroglia marker, myelin basic protein

In the central nervous system, oligodendrocytes are responsible for the production of myelin that serves to insulate the neuronal axons. Besides their role in myelin production, oligodendroglia also exhibit functional interaction with the endothelium and microglial cells (Miyamoto et al. 2014; Peferoen et al. 2014), thus associating with injury- or disease-related pathological changes. Here, we specifically examined the expression of the oligodendrocyte marker, myelin basic protein (MBP), to determine if oligodendroglia associate themselves with neuronal injury. Expression of MBP was assessed by western immunoblot analysis.

Exposure to the low-dose FSD 8 aerosol did not affect MBP protein content in the STR (Fig. 18 and S5C) and CER (Fig. 18 and S5D). However, a large increase in MBP protein content (90.5%) was seen in the OB (Fig. 18 and S5A) at 7 d post-exposure. Increased MBP protein content (29.8%) was also seen in the HIP (Fig. 18 and S5B) at 7 d that recovered to control levels by 27 d.

Exposure to the high dose of FSD 8 caused a time-dependent reduction in MBP in the OB (Fig. 18 and S5A) at 7 d (20.8% decrease; not statistically significant), 27 d (38.5% decrease) and 90 d (44.5% decrease) post-exposure, respectively. In the HIP (Fig. 18 and S5B), the high dose FSD 8 caused an early reduction in MBP levels (42% decrease) by 1 d, after which the levels increased (70% and 36%) at 7 d and 27 d before recovering to control values at 90 d. In the STR (Fig. 18 and S5C), MBP content was unaffected by the high dose FSD 8 treatment. In the CER (Fig. 18 and S5D), the high dose of FSD 8 caused a transient reduction in MBP content (27.5% decrease) at 7 d that recovered to control values by 27 d and remained unchanged at 90 d.

4. Discussion

There is emerging concern that workers at hydraulic fracturing well sites may be exposed to FSDs generated during the transportation and handling of sand proppants. FSDs are generally composed of crystalline silica containing particles in the respirable range. Field investigations conducted by NIOSH have shown that the levels of FSDs at well sites can exceed the permissible exposure limits established for crystalline silica (Esswein et al. 2013). While there is substantial information on the health effects of crystalline silica *per se*, there is very little information on the toxicological effects of FSDs, including those pertaining to the nervous system. Although FSD 8 was composed primarily of crystalline silica (Fedan et al. 2020), other naturally-occurring elements, such as Al, K, Ca, Mg, Mn, Fe and Co are present in the dust. While the needed information is not known at present, it is

worth considering whether the observed neurotoxicological responses could be attributable to the nonsilica elements in the dust, to crystalline silica that made up the bulk of the dust particles, or to both.

Our low dose and high dose rodent model mimic an FSD exposure paradigm of ~0.66 or 2 years in a worker (Russ et al. 2020), respectively, if exposure were to occur at 10-fold higher rate than the NIOSH REL (0.05 mg/m^3 TWA for crystalline silica). Such high levels of silica dusts have been previously reported at well sites where fracking was used (Esswein et al. 2013). While this exposure scenario may not be reflective of the multiple years of exposure that a worker may encounter at the workplace, it represents an acute paradigm during which early signs of an abnormality, injury or damage can be detected, particularly to the nervous system. This may provide scope for developing early detection, intervention and/or prevention strategies.

We have shown previously that repeated pulmonary exposure of rats to metal particulates derived from welding caused neuroinflammation and neurotoxicity (Sriram et al. 2010a, 2014). Exposure to FSD 8 aerosol, particularly at the lower dose, elicited neuroinflammation, as evidenced by increased expression of mRNAs for arachidonate 5-lipoxygenase (*Alox5/5-LO*), prostaglandin-endoperoxide synthase 1 (*Ptgs1/Cox1*), prostaglandin-endoperoxide synthase 2 (*Ptgs2/Cox2*), nitric oxide synthase 2 (*Nos2/iNos*), IL-6 (*Il6*) and TNFα (*Tnfa*) in the brain areas examined. Early changes in the mRNA expression of *Alox5, Ptgs1* and *Ptgs2*, key intermediaries in the arachidonic acid pathway, were observed. On the other hand, the expressions of *Il6*, *Tnfa* and *Nos2* mRNAs exhibited delayed responses. Increased levels of arachidonic acid have been linked to neuroinflammation, and high levels of arachidonic acid have been found in the brain following ischemia, seizure, hypoxia and hypoglycaemia (Phillis et al. 2006).

Concurrent with neuroinflammation, FSD 8 aerosols also altered the mRNA expression of *Mmp9, Cldn1* and *Cldn3*, which are markers that are associated with BBB integrity and vascular blood flow. Claudins are cell adhesion molecules of tight junctions that are critical for the formation of the BBB. The expression of *Mmp9, Cldn1* and *Cldn3* at the BBB has been reported (Bazzoni and Dejana 2004). Generally, reductions in the expression of claudins is known to be associated with a reduction in BBB permeability (Kniesel and Wolburg 2000; Ueno et al. 2004). *Cldn1* is an integral component of the tight junctions and its loss is associated with several brain pathologies, including stroke and brain tumor, as well as brain inflammatory diseases (Liebner et al. 2000). Indeed, inflammation with release of arachidonic acid or inflammatory mediators like *Nos2, Il6*, *Tnfa* and interferon-γ (*Ifng*) has been linked to increased permeability and breakdown of the BBB (Brooks et al. 2005; Lopez-Ramirez et al. 2012). Arachidonic acid, in particular, can induce lesions in endothelial cells, mediate vasogenic edema, cause cerebral arteriolar damage, and elicit secondary brain injury (Kontos et al. 1980; Wahl et al., 1988).

With the exception of quartz, all tectosilicate minerals are aluminosilicates. The tectosilicate minerals, microcline and orthoclase, are the most abundant group of alkali feldspars and make up nearly 40% of the earth's crust. Aluminosilicate clay minerals like kaolin have been shown to cause axonal damage, disrupt axonal and synaptic connections, alter dendritic

architecture, elicit glial activation, and lead to enlargement of ventricles (Harriset al., 1996; Del Bigio et al. 1997). Exposure to respirable geogenic dusts containing mixtures of crystalline silica, silicate minerals, as well as other naturally-occurring metals like Al, Fe, Mn and arsenic has been shown to elicit immunological changes in laboratory animals (Keil et al. 2016a, 2016b) and at higher doses reduce myelin immunoreactivity (DeWitt et al., 2017). Exposure to lunar and Martian dusts have also been shown to modulate brain glutamate homeostasis (Krisanova et al. 2013). These studies indicate the possibility of neurotoxic outcomes from inhaled mineral-sand dust exposures. In agreement with the above findings, our results define alterations in the protein levels of MBP, SYP, SYT and GFAP in various brain areas; however, a dose-dependent response relationship was not evident in many cases. Further, some of these effects were transient, exhibiting either an increase or decrease in protein expression.

A noteworthy observation was the persistent down-regulation of MBP in the OB, and of the neuronal synaptic proteins, SYP and SYT, in the CER after FSD 8 exposure, which are suggestive of perturbations in axonal and synaptic architecture. SYP and SYT are critical players in the exocytosis of synaptic vesicles, neurotransmitter release and synaptic plasticity. Multiple synaptic vesicle proteins are involved in neurotransmitter transport and release (Lin and Schellar, 2000; Jahn and Scheller 2006). The efficacy of synaptic transmission depends on a very complex and intricate coordination of various synaptic proteins and their plasticity (Murthy and DeCamilli, 2003; Kennedy et al. 2005). SYP is widely expressed in the brain (Marqueze-Pouey et al. 1991), particularly at the presynaptic terminals, and is involved in mediating the exocytosis-endocytosis of synaptic vesicles, as well as in regulating the assembly of the soluble N-ethylmaleimide-sensitive factor (NSF) attachment protein receptors (SNAREs) complex formation (Valtorta et al. 2004). Overexpression of SYP has been shown to enhance neurotransmitter release (Alder et al. 1995). Conversely, reduced SYP levels, as observed in this study, can impair neurotransmitter release. These observations suggest that perturbation of synaptic protein expression can contribute to synaptic dysfunction that is typically associated with neural injury and neurodegenerative disorders. Synaptic damage, synaptic loss and/or impaired synaptic plasticity are often associated with the functional decline of the nervous system. It is to be noted that no functional changes were observed in this study, perhaps due to the acute exposure duration. Generally, in neurological disorders, there is a latency between exposure and appearance of functional/clinical symptoms. Thus, it is likely that even the 90 d post-exposure duration is a relatively short period for appearance of any observable neurobehavioral or neurological deficits.

Concomitant with these neuronal perturbations, GFAP expression was increased, which is an index of glial cell activation. These FSD 8-induced changes are akin to some of the neural effects induced by kaolin. Kaolin also interacts with and/or affects various neurotransmitter systems, such as adrenergic, dopaminergic, and serotonergic, cholinergic and GABAergic (Miwa et al. 1982; Chovanes et al. 1988; Del Bigio and Vriend 1998). Our findings of altered biogenic amine neurotransmitters in discrete brain areas, especially after exposure to the low dose of FSD 8, are consistent with these reports. The imbalance in the levels of biogenic amines observed in various brain areas occurred early post-exposure and was transient, recovering to baseline values following withdrawal from exposure. The presence

of large amounts of crystalline silica, or the tectosilicate minerals, microcline and orthoclase, that are present in the FSD 8 aerosol, may have contributed to some of the neurotoxic effects.

Particle size characterization (Russ et al. 2020) revealed that the FSD 8 aerosol exhibited a mass median aerodynamic diameter (MMAD) of 1.75 μm. Scanning electron microscopy (SEM) analysis revealed the prevalent particle size range to be 0.5–1 μm. In addition, small amounts of nanoscale size FSD 8 particulates were also observed by SEM analysis. Recently, it has been shown that neurons can internalize micron-sized silicon dioxide (SiO_2) microspheres (Wallace et al. 2017). Previous studies have shown that silica nanoparticles (SiNPs) can translocate to the brain following intranasal instillation and cause inflammation, oxidative stress and reduced dopamine content in the striatum (Wu et al. 2011). SiNPs have also been shown to be internalized by human and mouse cell lines resulting in oxidative stress, apoptosis, increased amyloid β, tau phosphorylation, altered cellular morphology, reduced neuronal differentiation, as well as decreased cell viability (Yang et al. 2014; Ducray et al. 2017). More recently, it has been demonstrated that amorphous SiNPs can also translocate to the brain and cause synaptic, as well as neurobehavioral changes (You et al. 2018). While silica deposition was not directly examined in the nasal or brain regions in the current hazard identification study, the molecular changes in OB and CER suggest that these responses may be elicited by FSD 8 silica particulates that are transported to the brain.

Collectively, our findings suggest that FSD 8 exposure can elicit neuroinflammation and cause long-term axonal and synaptic changes. In general, we observed that the neuroinflammatory responses predominantly occurred at the lower dose of FSD 8, but at the higher dose there was a lack of an inflammatory response and in some cases even an inhibition/down-regulation of the response. Further, the higher dose of FSD 8 inhibited or reduced the expression of various neural proteins. Such effects were not only brain region- and time-dependent outcomes, but also unique to certain biological parameters. Cellular defense mechanisms and adaptive responses can often be triggered by low-dose exposures and inhibited at higher doses. The early and acute neuroinflammatory responses seen with the low dose of FSD 8, which resolves with time, could likely be a beneficial or neuroprotective response, while the inhibition of neural proteins by a high dose of FSD 8 may relate to a toxic effect. Whether such molecular aberrations will progressively culminate in neurodegeneration-like pathological changes remains unknown. Further, it needs to be determined if such effects follow direct FSD 8 particulate translocation to the brain or are mediated by indirect neurogenic/systemic mechanisms. It is to be noted that the FSD 8 sample investigated in this study may not be representative of all the sand proppants used in hydraulic fracturing. Indeed, the FSDs collected from nine drilling sites were found to be quite different mineralogically (Fedan et al. 2020). Additional studies are warranted to address these knowledge gaps, particularly to (i) establish an extensive dose-response profile that will be useful for neurological risk assessment, (ii) determine the long-term neurotoxic outcomes, including the potential for causing neurodegeneration akin to Parkinson’s or Alzheimer’s diseases, and (iii) determine if the long-term effects can be reversed with appropriate intervention.

Supplementary Material

Refer to Web version on PubMed Central for supplementary material.

Acknowledgments

Funding source

This study was funded by an intramural project (7927ZLDC) from the National Institute for Occupational Safety and Health.

Abbreviations:

5-HIAA	5-hydroxyindole-3-acetic acid
5-HT	5-hydroxytryptamine (serotonin)
AA	arachidonic acid
Actb	β-actin
Alox5	arachidonate 5-lipoxygenase (5-LO)
cDNA	complementary deoxyribonucleic acid
CER	cerebellum
Cldn1	claudin 1
Cldn3	claudin 3
DA	dopamine (3,4-dihydroxyphenethylamine)
DOPAC	3,4-dihydroxyphenylacetic acid
EPI	epinephrine
FCT	frontal cortex
FSD	fracking sand dust
GABA	γ-amino butyric acid
GFAP	glial fibrillary acidic protein
HIP	hippocampus
HPLC-EC	high performance liquid chromatography with electrochemical detection
HVA	homovanillic acid
Il6	interleukin 6
Ltc4s	leukotriene C4 synthase

MBP	myelin basic protein
MMAD	mass median aerodynamic diameter
mRNA	messenger ribonucleic acid
Mmp9	matrix metallopeptidase 9 (matrix metalloproteinase 9, gelatinase B)
NE	norepinephrine
Nos2	nitric oxide synthase 2 (inducible nitric oxide synthase iNOS)
OB	olfactory bulb
PBST	phosphate-buffered saline with Triton X-100
PCR	polymerase chain reaction
Pla2g2d	phospholipase A2 group IID (phospholipase A2, PLA2)
Ptgs1	prostaglandin-endoperoxide synthase 1 (cyclooxygenase 1, COX1)
Ptgs2	prostaglandin-endoperoxide synthase 2 (cyclooxygenase 2, COX2)
PVDF	polyvinylidene fluoride
REL	recommended exposure limit
RNA	ribonucleic acid
SEM	scanning electron microscopy
STR	striatum
SYP	synaptophysin
SYT	synaptotagmin 1
Tnf	tumor necrosis factor
YWHAE	tyrosine 3-monooxygenase/tryptophan 5-monooxygenase activation protein-ε (14–3-3-ε)

References

Alder J, Kanki H, Valtorta F, Greengard P, Poo MM, 1995 Overexpression of synaptophysin enhances neurotransmitter secretion at Xenopus neuromuscular synapses. J. Neurosci 15, 511–519. [PubMed: 7823159]

Allen NJ, 2014 Astrocyte regulation of synaptic behavior. Annu. Rev. Cell Dev. Biol 30, 439–463. [PubMed: 25288116]

Allen JL, Liu X, Weston D, Prince L, Oberdörster G, Finkelstein JN, Johnston CJ, Cory-Slechta DA, 2014 Developmental exposure to concentrated ambient ultrafine particulate matter air pollution in mice results in persistent and sex-dependent behavioral neurotoxicity and glial activation. Toxicol. Sci 140, 160–178. [PubMed: 24690596]

Anderson SE, Shane H, Long C, Marrocco A, Lukomska E, Roberts JR, Marshall N, Fedan JS, 2020 Biological effects of inhaled hydraulic fracturing sand dust. VIII. Immunotoxicity. Toxicol Appl

Pharmacol 408, 115256 10.1016/j.taap.2020.115256 (9 30, Epub ahead of print. PMID: 33007384). [PubMed: 33007384]

Bazzoni G, Dejana E, 2004 Endothelial cell-to-cell junctions: molecular organization and role in vascular homeostasis. Physiol. Rev 84, 869–901. [PubMed: 15269339]

Brooks TA, Hawkins BT, Huber JD, Egleton RD, Davis TP, 2005 Chronic inflammatory pain leads to increased blood-brain barrier permeability and tight junction protein alterations. Am. J. Physiol. Heart Circ. Physiol 289, H738–H743. [PubMed: 15792985]

Calderon-Garciduenas L, Valencia-Salazar G, Rodriguez-Alcaraz A, Gambling TM, Garcia R, Osnaya N, Villarreal-Calderon A, Devlin RB, Carson JL, 2001 Ultrastructural nasal pathology in children chronically and sequentially exposed to air pollutants. Am. J. Respir. Cell Mol. Biol 24, 132–138. [PubMed: 11159046]

Calderon-Garciduenas L, Maronpot RR, Torres-Jardon R, Henriquez-Roldan C, Schoonhoven R, Acuna-Ayala H, Villarreal-Calderon A, Nakamura J, Fernando R, Reed W, Azzarelli B, Swenberg JA, 2003 DNA damage in nasal and brain tissues of canines exposed to air pollutants is associated with evidence of chronic brain inflammation and neurodegeneration. Toxicol. Pathol 31, 524–538. [PubMed: 14692621]

Calderon-Garciduenas L, Reed W, Maronpot RR, Henriquez-Roldan C, Delgado-Chavez R, Calderon-Garciduenas A, Dragustinovis I, Franco-Lira M, Aragon-Flores M, Solt AC, Altenburg M, Torres-Jardon R, Swenberg JA, 2004 Brain inflammation and Alzheimer's-like pathology in individuals exposed to severe air pollution. Toxicol. Pathol 32, 650–658. [PubMed: 15513908]

Calderon-Garciduenas L, Franco-Lira M, Torres-Jardon R, Henriquez-Roldan C, Barragan-Mejia G, Valencia-Salazar G, Gonzalez-Maciel A, Reynoso-Robles R, Villarreal-Calderon R, Reed W, 2007 Pediatric respiratory and systemic effects of chronic air pollution exposure: nose, lung, heart, and brain pathology. Toxicol. Pathol. 35, 154–162. [PubMed: 17325984]

Chovanes GI, McAllister JP 2nd, Lamperti AA, Salotto AG, Truex RC Jr., 1988 Monoamine alterations during experimental hydrocephalus in neonatal rats. Neurosurgery 22, 86–91. [PubMed: 3344092]

Del Bigio MR, Vriend JP, 1998 Monoamine neurotransmitters and amino acids in the cerebrum and striatum of immature rats with kaolin-induced hydrocephalus. Brain Res. 798, 119–126. [PubMed: 9666099]

Del Bigio MR, Kanfer JN, Zhang YW, 1997 Myelination delay in the cerebral white matter of immature rats with kaolin-induced hydrocephalus is reversible. J. Neuropathol. Exp. Neurol 56, 1053–1066. [PubMed: 9291946]

DeWitt JC, Buck BJ, Goossens D, Teng Y, Pollard J, McLaurin BT, Gerads R, Keil DE, 2017 Health effects following subacute exposure to geogenic dust collected from active drainage surfaces (Nellis dunes recreation area, Las Vegas, NV). Toxicol. Rep 4, 19–31. [PubMed: 28959621]

Ducray AD, Stojiljkovic A, Moller A, Stoffel MH, Widmer HR, Frenz M, Mevissen M, 2017 Uptake of silica nanoparticles in the brain and effects on neuronal differentiation using different in vitro models. Nanomedicine 13, 1195–1204. [PubMed: 27871963]

Esswein EJ, Breitenstein M, Snawder J, Kiefer M, Sieber WK, 2013 Occupational exposures to respirable crystalline silica during hydraulic fracturing. J. Occup. Environ. Hyg 10, 347–356. [PubMed: 23679563]

Farhy-Tselnicker I, Allen NJ, 2018 Astrocytes, neurons, synapses: a tripartite view on cortical circuit development. Neural. Dev 13 (1), 7 (5 1). [PubMed: 29712572]

Fedan JS, 2020 Biological effects of inhaled hydraulic fracturing sand dust. I. Scope of the investigation. Toxicol Appl Pharmacol (manuscript submitted to this journal as a tandem paper to accompany this manuscript.).

Fedan JS, Hubbs AF, Barger M, Schwegler-Berry D, Friend S, Leonard SS, Thompson JA, Jackson MC, Snawder JE, Dozier AK, Coyle J, Kashon ML, Park JH, Mckinney W, Roberts JR, 2020 Biological effects of inhaled hydraulic fracturing sand dust. II. Particle characterization and pulmonary effects 30 d following intratracheal instillation. Toxicol Appl Pharmacol. 10.1016/j.taap.2020.115282 (Epub ahead of print. PMID: 33068622).

Harris NG, McAllister JP 2nd, Conaughty JM, Jones HC, 1996 The effect of inherited hydrocephalus and shunt treatment on cortical pyramidal cell dendrites in the infant H-Tx rat. Exp. Neurol 141, 269–279. [PubMed: 8812160]

Huber JD, Egleton RD, Davis TP, 2001 Molecular physiology and pathophysiology of tight junctions in the blood-brain barrier. Trends Neurosci. 24, 719–725. [PubMed: 11718877]

Hunot S, Hartmann A, Hirsch EC, 2001 The inflammatory response in the Parkinson brain. Clin. Neurosci. Res 1, 434–443. 10.1016/S1566-2772(01)00022-6.

Jahn R, Scheller RH, 2006 SNAREs–engines for membrane fusion. Nat Rev Mol Cell Biol 7, 631–643. [PubMed: 16912714]

Keil D, Buck B, Goossens D, Teng Y, Leetham M, Murphy L, Pollard J, Eggers M, McLaurin B, Gerads R, DeWitt J, 2016a Immunotoxicological and neurotoxicological profile of health effects following subacute exposure to geogenic dust from sand dunes at the Nellis dunes recreation area, Las Vegas, NV. Toxicol. Appl. Pharmacol 291, 1–12. [PubMed: 26644169]

Keil DE, Buck B, Goossens D, Teng Y, Pollard J, McLaurin B, Gerads R, DeWitt J, 2016b Health effects from exposure to atmospheric mineral dust near Las Vegas, NV, USA. Toxicol. Rep 3, 785–795. [PubMed: 28959605]

Kennedy MB, Beale HC, Carlisle HJ, Washburn LR, 2005 Integration of biochemical signalling in spines. Nat. Rev. Neurosci 6, 423–434. [PubMed: 15928715]

Kniesel U, Wolburg H, 2000 Tight junctions of the blood-brain barrier. Cell. Mol. Neurobiol 20, 57–76. [PubMed: 10690502]

Kontos HA, Wei EP, Povlishock JT, Dietrich WD, Magiera CJ, Ellis EF, 1980 Cerebral arteriolar damage by arachidonic acid and prostaglandin G2. Science 209, 1242–1245. [PubMed: 7403881]

Kreutzberg GW, 1996 Microglia: a sensor for pathological events in the CNS. Trends Neurosci. 19, 312–318. [PubMed: 8843599]

Krisanova N, Kasatkina L, Sivko R, Borysov A, Nazarova A, Slenzka K, Borisova T, 2013 Neurotoxic potential of lunar and martian dust: influence on em, proton gradient, active transport, and binding of glutamate in rat brain nerve terminals. Astrobiology 13, 679–692. [PubMed: 23919751]

Liebner S, Fischmann A, Rascher G, Duffner F, Grote EH, Kalbacher H, Wolburg H, 2000 Claudin-1 and claudin-5 expression and tight junction morphology are altered in blood vessels of human glioblastoma multiforme. Acta Neuropathol. 100, 323–331. [PubMed: 10965803]

Lin RC, Scheller RH, 2000 Mechanisms of synaptic vesicle exocytosis. Annu. Rev. Cell Dev. Biol 16, 19–49. [PubMed: 11031229]

Lopez-Ramirez MA, Fischer R, Torres-Badillo CC, Davies HA, Logan K, Pfizenmaier K, Male DK, Sharrack B, Romero IA, 2012 Role of caspases in cytokine-induced barrier breakdown in human brain endothelial cells. J. Immunol 189, 3130–3139. [PubMed: 22896632]

Marqueze-Pouey B, Wisden W, Malosio ML, Betz H, 1991 Differential expression of synaptophysin and synaptoporin mRNAs in the postnatal rat central nervous system. J. Neurosci 11, 3388–3397. [PubMed: 1941089]

McGeer PL, McGeer EG, 2004 Inflammation and neurodegeneration in Parkinson's disease. Parkinsonism Relat. Disord. 10 (Suppl. 1), S3–S7. [PubMed: 15109580]

McKinney W, Chen B, Schwegler-Berry D, Frazer DG, 2013 Computer-automated silica aerosol generator and animal inhalation exposure system. Inhal. Toxicol 25, 363–372. [PubMed: 23796015]

Miwa S, Inagaki C, Fujiwara M, Takaori S, 1982 The activities of noradrenergic and dopaminergic neuron systems in experimental hydrocephalus. J. Neurosurg 57, 67–73. [PubMed: 7086502]

Miyamoto N, Pham LD, Seo JH, Kim KW, Lo EH, Arai K, 2014 Crosstalk between cerebral endothelium and oligodendrocyte. Cell. Mol. Life Sci 71, 1055–1066. [PubMed: 24132511]

Mogi M, Harada M, Riederer P, Narabayashi H, Fujita K, Nagatsu T, 1994 Tumor necrosis factor-alpha (TNF-alpha) increases both in the brain and in the cerebrospinal fluid from parkinsonian patients. Neurosci. Lett 165, 208–210. [PubMed: 8015728]

Murthy VN, De Camilli P, 2003 Cell biology of the presynaptic terminal. Annu. Rev. Neurosci 26, 701–728. [PubMed: 14527272]

Oberdörster G, Sharp Z, Atudorei V, Elder A, Gelein R, Kreyling W, Cox C, 2004 Translocation of inhaled ultrafine particles to the brain. Inhal. Toxicol 16, 437–445. [PubMed: 15204759]

Olgun NS, Morris AM, Stefaniak AB, Bowers LN, Knepp AK, Duling MG, Mercer RR, Kashon ML, Fedan JS and Leonard SS, 2020 Biological effects of inhaled hydraulic fracturing sand dust. III. Cytotoxicity and pro-inflammatory responses in cultured murine macrophage cells. *Toxicol Appl Pharmacol* (manuscript submitted to this journal as a tandem paper to accompany this manuscript).

Peferoen L, Kipp M, van der Valk P, van Noort JM, Amor S, 2014 Oligodendrocyte-microglia cross-talk in the central nervous system. Immunology 141, 302–313. [PubMed: 23981039]

Phillis JW, Horrocks LA, Farooqui AA, 2006 Cyclooxygenases, lipoxygenases, and epoxygenases in CNS: their role and involvement in neurological disorders. Brain Res. Rev 52, 201–243. [PubMed: 16647138]

Russ KA, Thompson JA, Reynolds JS, Roberts JR, Mercer RR, Porter DW, McKinney W, Dey RD, Barger M, Cumpston J, Batchelor TP, Kashon ML, Kodali V, Sriram K, Fedan JS, 2020 Biological effects of inhaled hydraulic fracturing sand dust. IV. Pulmonary effects. Toxicol Appl Pharmacol. 10.1016/j.taap.2020.115284 (Epub ahead of print. PMID: 33068619).

Sager TM, Roberts JR, Umbright CM, Barger M, Kashon ML, Fedan JS, Joseph P, 2020 Biological effects of inhaled hydraulic fracturing sand dust. V. Pulmonary inflammatory, cytotoxic and oxidant effects. Toxicol Appl Pharmacol 408, 115280 10.1016/j.taap.2020.115280 (Epub ahead of print. PMID: 33065154). [PubMed: 33065154]

Sriram K, Matheson JM, Benkovic SA, Miller DB, Luster MI, O'Callaghan JP, 2002 Mice deficient in TNF receptors are protected against dopaminergic neurotoxicity: implications for Parkinson's disease. FASEB J. 16, 1474–1476. [PubMed: 12205053]

Sriram K, Matheson JM, Benkovic SA, Miller DB, Luster MI, O'Callaghan JP, 2006a Deficiency of TNF receptors suppresses microglial activation and alters the susceptibility of brain regions to MPTP-induced neurotoxicity: role of TNF-alpha. FASEB J. 20, 670–682. [PubMed: 16581975]

Sriram K, Miller DB, O'Callaghan JP, 2006b Minocycline attenuates microglial activation but fails to mitigate striatal dopaminergic neurotoxicity: role of tumor necrosis factor-alpha. J. Neurochem 96, 706–718. [PubMed: 16405514]

Sriram K, Lin GX, Jefferson AM, Roberts JR, Chapman RS, Chen BT, Soukup JM, Ghio AJ, Antonini JM, 2010a Dopaminergic neurotoxicity following pulmonary exposure to manganese-containing welding fumes. Arch. Toxicol 84, 521–540. [PubMed: 20224926]

Sriram K, Lin GX, Jefferson AM, Roberts JR, Wirth O, Hayashi Y, Krajnak KM, Soukup JM, Ghio AJ, Reynolds SH, Castranova V, Munson AE, Antonini JM, 2010b Mitochondrial dysfunction and loss of Parkinson's disease-linked proteins contribute to neurotoxicity of manganese-containing welding fumes. FASEB J. 24, 4989–5002. [PubMed: 20798247]

Sriram K, Jefferson AM, Lin GX, Afshari A, Zeidler-Erdely PC, Meighan TG, McKinney W, Jackson M, Cumpston A, Cumpston JL, Leonard HD, Frazer DG, Antonini JM, 2014 Neurotoxicity following acute inhalation of aerosols generated during resistance spot weld-bonding of carbon steel. Inhal. Toxicol 26, 720–732. [PubMed: 25265048]

Streit WJ, Walter SA, Pennell NA, 1999 Reactive microgliosis. Prog. Neurobiol 57, 563–581. [PubMed: 10221782]

Stringfellow WT, Camarillo MK, Domen JK, Sandelin WL, Varadharajan C, Jordan PD, Reagan MT, Cooley H, Heberger MG, Birkholzer JT, 2017 Identifying chemicals of concern in hydraulic fracturing fluids used for oil production. Environ. Pollut 220, 413–420. [PubMed: 27743793]

Investigative Team, 2020 Biological effects of inhaled hydraulic fracturing sand dust. IX. Summary and significance. *Toxicol Appl Pharmacol* (manuscript submitted to this journal as a tandem paper to accompany this manuscript).

Thiel VE, Audus KL, 2001 Nitric oxide and blood-brain barrier integrity. Antioxid. Redox Signal 3, 273–278. [PubMed: 11396481]

Tin Tin Win S, Mitsushima D, Yamamoto S, Fukushima A, Funabashi T, Kobayashi T, Fujimaki H, 2008 Changes in neurotransmitter levels and proinflammatory cytokine mRNA expressions in the mice olfactory bulb following nanoparticle exposure. Toxicol. Appl. Pharmacol 226, 192–198. [PubMed: 17950771]

Ueno M, Sakamoto H, Liao YJ, Onodera M, Huang CL, Miyanaka H, Nakagawa T, 2004 Blood-brain barrier disruption in the hypothalamus of young adult spontaneously hypertensive rats. Histochem. Cell Biol 122, 131–137. [PubMed: 15258771]

Valtorta F, Pennuto M, Bonanomi D, Benfenati F, 2004 Synaptophysin: leading actor or walk-on role in synaptic vesicle exocytosis? Bioessays 26, 445–453. [PubMed: 15057942]

Wahl M, Unterberg A, Baethmann A, Schilling L, 1988 Mediators of blood-brain barrier dysfunction and formation of vasogenic brain edema. J. Cereb. Blood Flow Metab 8, 621–634. [PubMed: 2843554]

Wallace VJ, Cimbro R, Rubio FJ, Fortuno LV, Necarsulmer JC, Koivula PP, Henderson MJ, DeBiase LM, Warren BL, Harvey BK, Hope BT, 2017 Neurons internalize functionalized Micron-sized silicon dioxide microspheres. Cell. Mol. Neurobiol 37, 1487–1499. [PubMed: 28260198]

Wu J, Wang C, Sun J, Xue Y, 2011 Neurotoxicity of silica nanoparticles: brain localization and dopaminergic neurons damage pathways. ACS Nano 5, 4476–4489. [PubMed: 21526751]

Yang X, He C, Li J, Chen H, Ma Q, Sui X, Tian S, Ying M, Zhang Q, Luo Y, Zhuang Z, Liu J, 2014 Uptake of silica nanoparticles: neurotoxicity and Alzheimer-like pathology in human SK-N-SH and mouse neuro2a neuroblastoma cells. Toxicol. Lett 229, 240–249. [PubMed: 24831964]

You R, Ho YS, Hung CH, Liu Y, Huang CX, Chan HN, Ho SL, Lui SY, Li HW, Chang RC, 2018 Silica nanoparticles induce neurodegeneration-like changes in behavior, neuropathology, and affect synapse through MAPK activation. Part Fibre Toxicol 15, 28. [PubMed: 29970116]

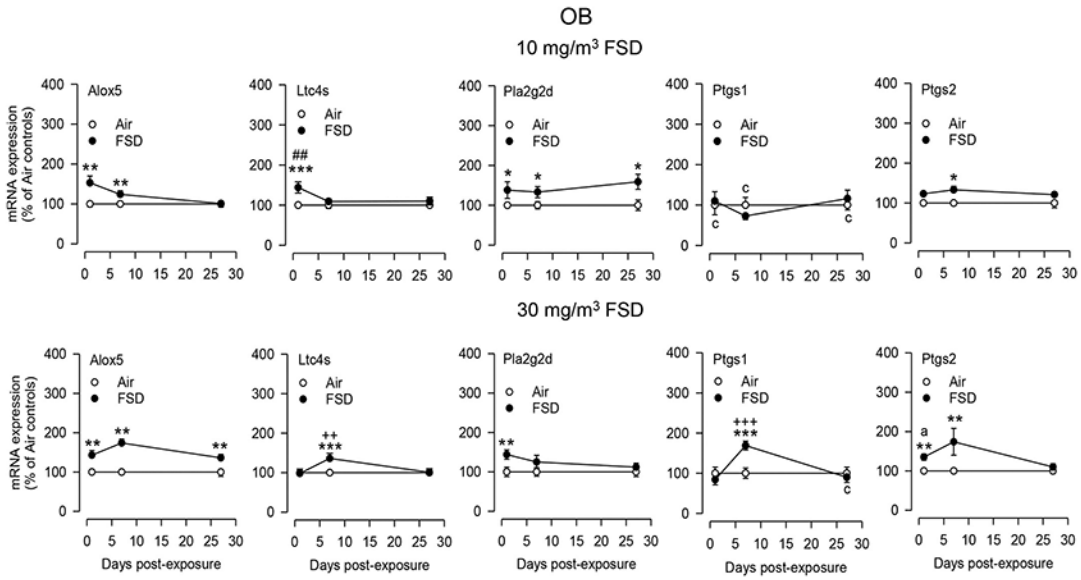

Fig. 1.

Expression of arachidonic acid pathway-associated genes in the olfactory bulb (OB). (FSD 8 is abbreviated as FSD in all the figures). Rats were exposed to FSD 8 aerosol (10 or 30 mg/m^3; 6 h/d × 4 d) by whole-body inhalation. At 1, 7 or 27 d post-exposure, the mRNA expression of *Alox5, Ltc4s, Pla2g2d, Ptgs1 and Ptgs2* were assayed by TaqMan real-time PCR. Following normalization to the endogenous control β-actin (*Actb*), the change in mRNA expression was calculated as percent of air-exposed controls. n = 5–6/group. ^{c}n = 5 due to one undetected sample in assay group; *P < 0.05, **P < 0.01, ***P < 0.001. $^{\#}$, $^{\#\#}$ or $^{\#\#\#}$ indicates values significantly different from the low dose FSD 8 at P < 0.05, 0.01 or 0.001, respectively. $^{+}$, $^{++}$ or $^{+++}$ indicates values significantly different from low dose FSD 8 at P < 0.05, 0.01 or 0.001, respectively.

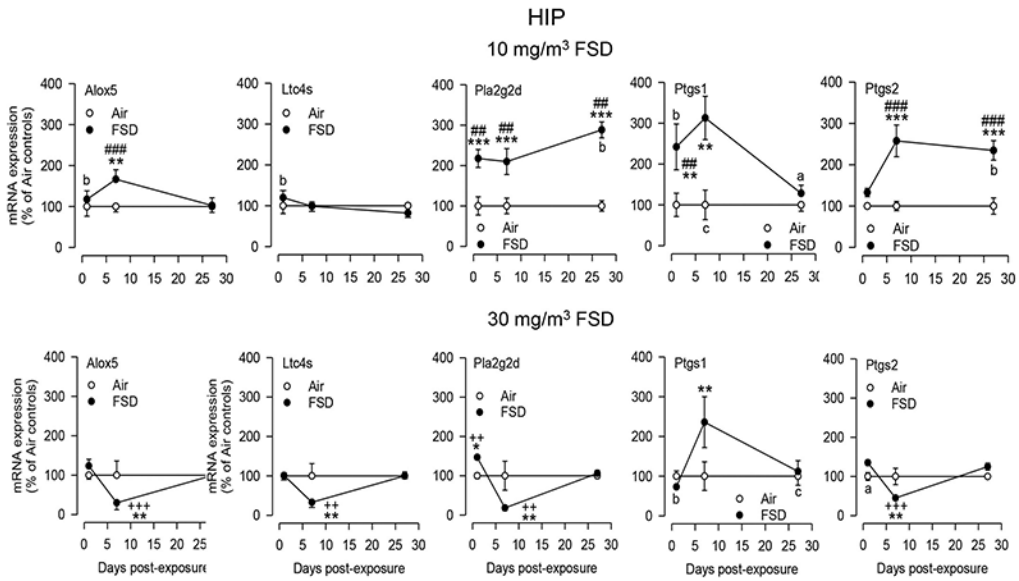

Fig. 2.

Expression of arachidonic acid pathway-associated genes in the hippocampus (HIP). Rats were exposed to FSD 8 aerosol (10 or 30 mg/m^3; 6 h/d × 4 d) by whole-body inhalation. At 1, 7 or 27 d post-exposure, the mRNA expression of *Alox5, Ltc4s, Pla2g2d*, *Ptgs1 and Ptgs2* were assayed by TaqMan real-time PCR. Following normalization to the endogenous control β-actin (*Actb*), the change in mRNA expression was calculated as percent of air-exposed controls. $n = 4$–6/group. $^a n = 5$ due to one outlier sample in assay group; $^b n = 4$ due to two outlier sample in assay group; $^c n = 5$ due to one undetected sample in assay group; $*P <$ 0.05, $**P < 0.01$, $***P < 0.001$. $^{\#}$, $^{\#\#}$ or $^{\#\#\#}$ indicates values significantly different from the high dose FSD 8 at $P < 0.05$, 0.01 or 0.001, respectively. $^{+}$, $^{++}$ or $^{+++}$ indicates values significantly different from the low dose of FSD 8 at $P < 0.05$, 0.01 or 0.001, respectively.

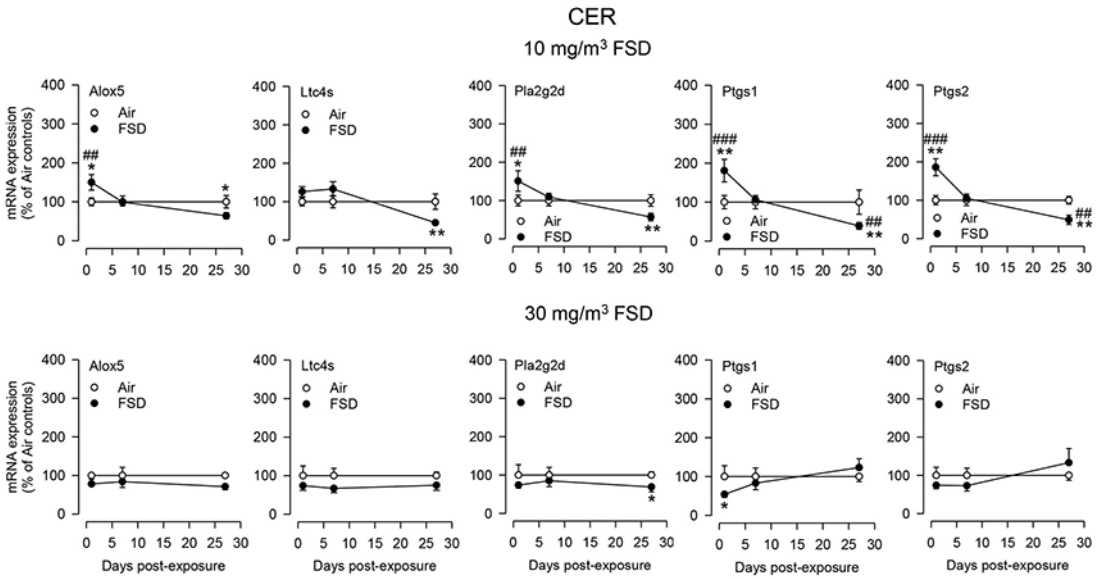

Fig. 3.

Expression of arachidonic acid pathway-associated genes in the cerebellum (CER). Rats were exposed to FSD 8 aerosol (10 or 30 mg/m^3; 6 h/d × 4 d) by whole-body inhalation. At 1, 7 or 27 d post-exposure, the mRNA expression of *Alox5, Ltc4s, Pla2g2d, Ptgs1 and Ptgs2* were assayed by TaqMan real-time PCR. Following normalization to the endogenous control β-actin (*Actb*), the change in mRNA expression was calculated as percent of air-exposed controls. $n = 6$/group. *$P < 0.05$, **$P < 0.01$, ***$P < 0.001$. $^{\#}$, $^{\#\#}$ or $^{\#\#\#}$ indicates values significantly different from the high dose FSD 8 at $P < 0.05$, 0.01 or 0.001, respectively. $^{+}$, $^{++}$ or $^{+++}$ indicates values significantly different from the low dose of FSD 8 at $P < 0.05$, 0.01 or 0.001, respectively.

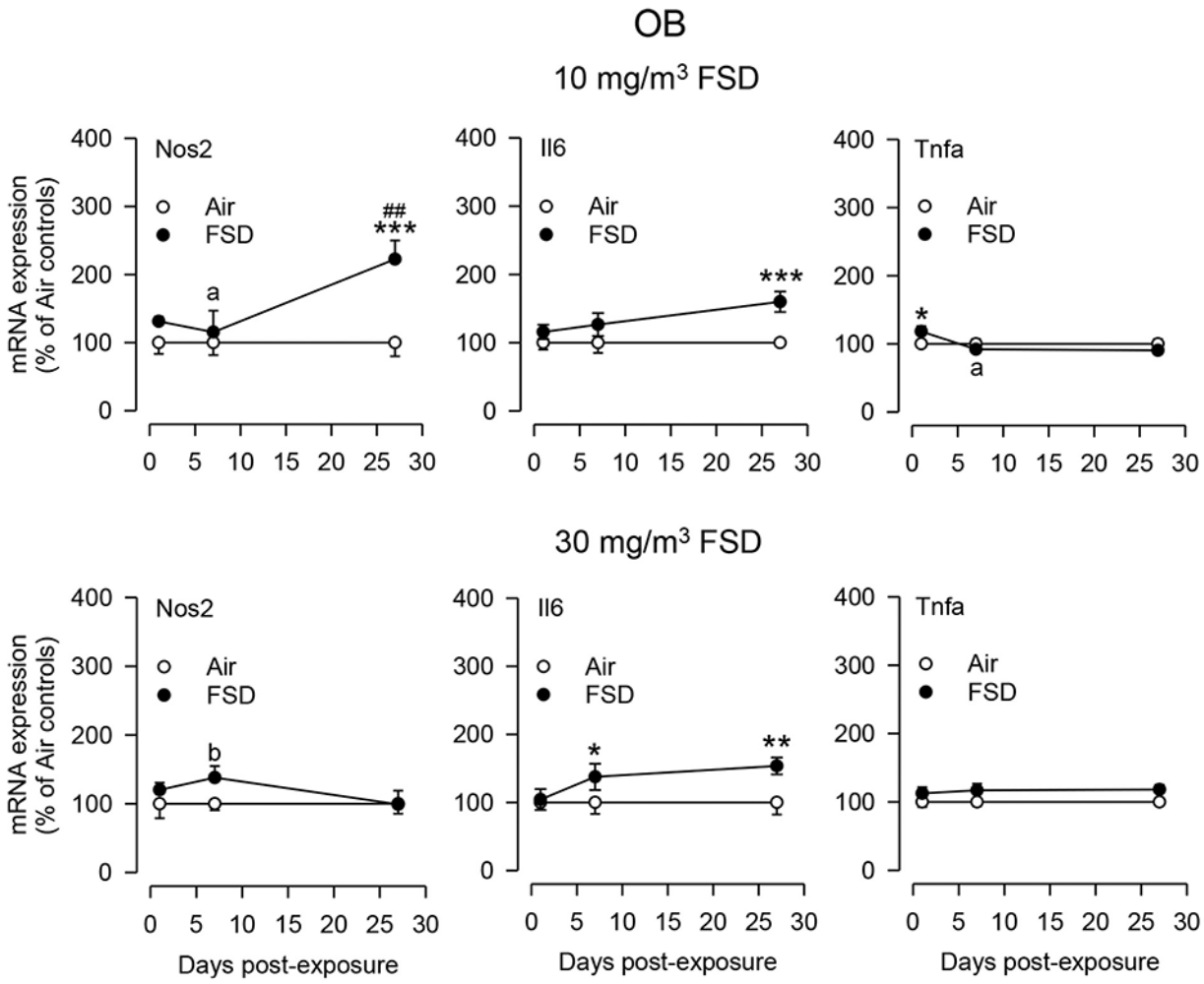

Fig. 4.

Expression of neuroinflammatory mediators in the olfactory bulb (OB). Rats were exposed to FSD 8 aerosol (10 or 30 mg/m^3; 6 h/d × 4 d) by whole-body inhalation. At 1, 7 or 27 d post-exposure, the mRNA expression of *Nos2*, *Il6* and *Tnfa* were assayed by TaqMan real-time PCR. Following normalization to the endogenous control β-actin (*Actb*), the change in mRNA expression was calculated as percent of air-exposed controls. n = 4–6/group. [a]n = 5 due to one outlier sample in assay group; [b]n = 4 due to two outlier sample in assay group; *P < 0.05, **P < 0.01, ***P < 0.001. [#], [##] or [###] indicates values significantly different from the high dose FSD 8 at P < 0.05, 0.01 or 0.001, respectively. [+], [++] or [+++] indicates values significantly different from the low dose of FSD 8 at P < 0.05, 0.01 or 0.001, respectively.

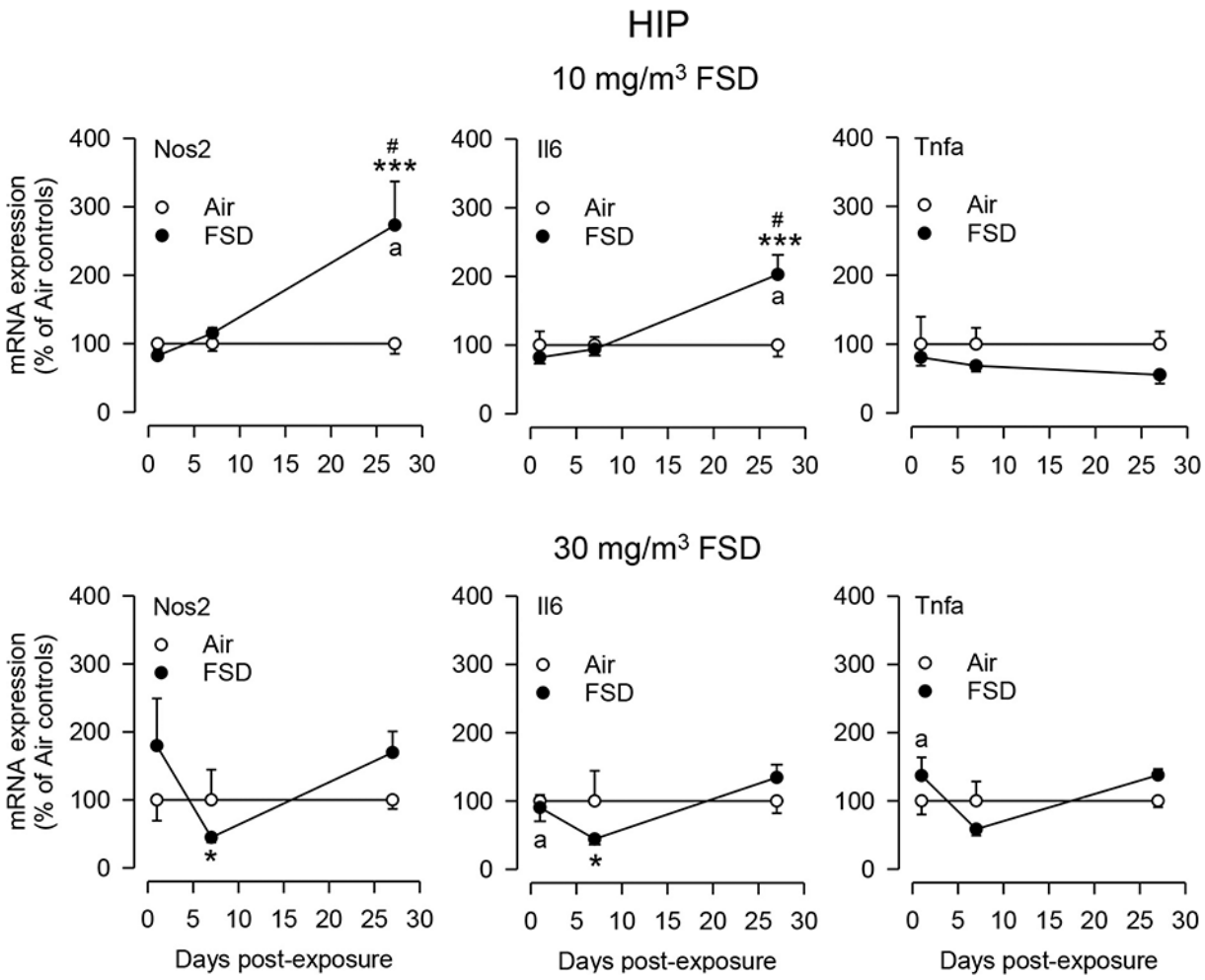

Fig. 5.

Expression of neuroinflammatory mediators in the hippocampus (HIP). Rats were exposed to FSD 8 aerosol (10 or 30 mg/m^3; 6 h/d × 4 d) by whole-body inhalation. At 1, 7 or 27 d post-exposure, the mRNA expression of *Nos2, Il6* and *Tnfa* were assayed by TaqMan real-time PCR. Following normalization to the endogenous control β-actin (*Actb*), the change in mRNA expression was calculated as percent of air-exposed controls. n = 5-6/group. [a]n = 5 due to one outlier sample in assay group; *P < 0.05, **P < 0.01, ***P < 0.001. [#], [##] or [###] indicates values significantly different from the high dose FSD 8 at P < 0.05, 0.01 or 0.001, respectively. [+], [++] or [+++] indicates values significantly different from the low dose of FSD 8 at P < 0.05, 0.01 or 0.001, respectively.

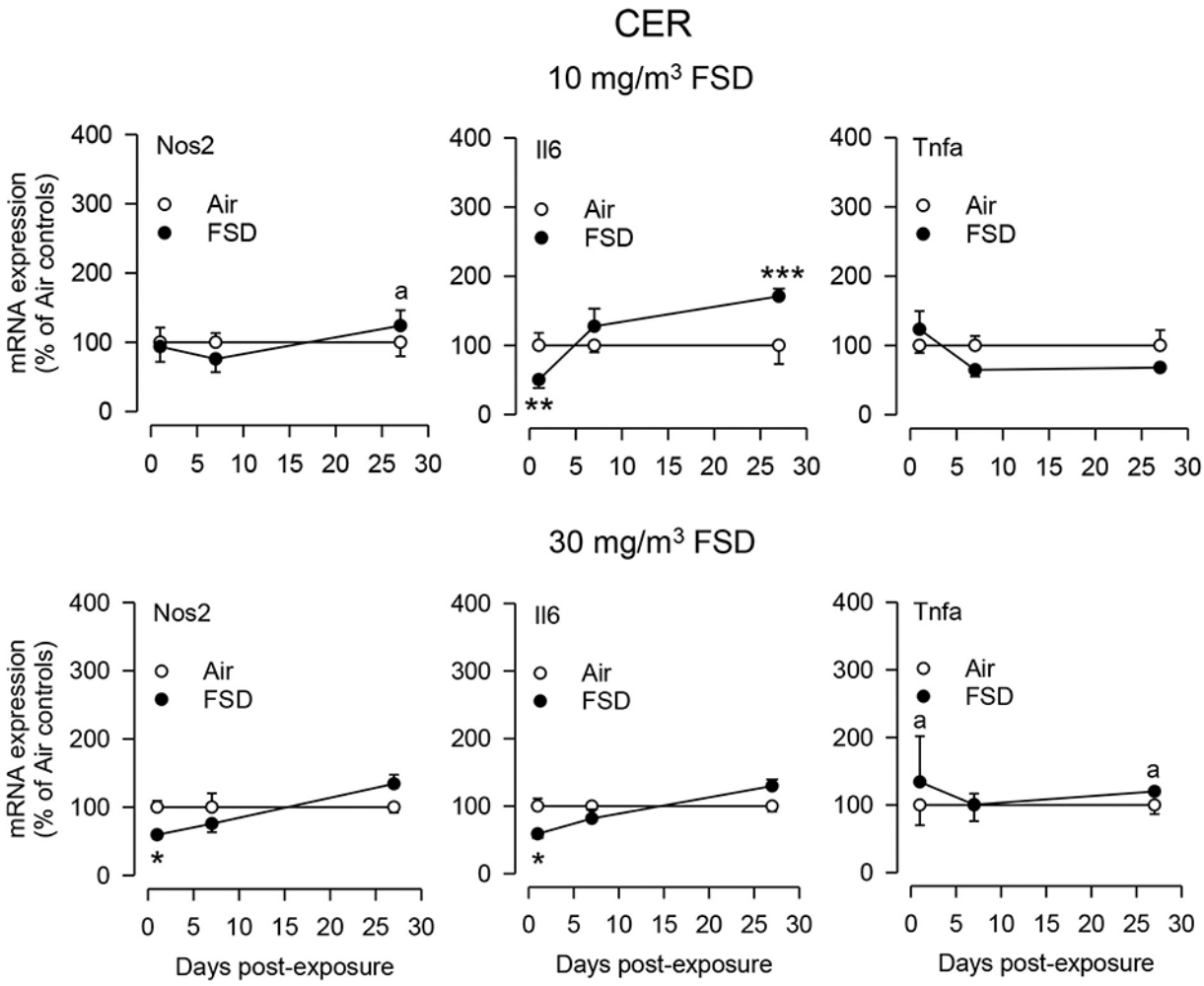

Fig. 6.

Expression of neuroinflammatory mediators in the cerebellum (CER). Rats were exposed to FSD 8 aerosol (10 or 30 mg/m^3; 6 h/d × 4 d) by whole-body inhalation. At 1, 7 or 27 d post-exposure, the mRNA expression of *Nos2*, *Il6* and *Tnfa* were assayed by TaqMan real-time PCR. Following normalization to the endogenous control β-actin (*Actb*), the change in mRNA expression was calculated as percent of air-exposed controls. n = 5-6/group. $^a n = 5$ due to one outlier sample in assay group; $^*P < 0.05$, $^{**}P < 0.01$, $^{***}P < 0.001$. $^{\#}$, $^{\#\#}$ or $^{\#\#\#}$ indicates values significantly different from the high dose FSD 8 at $P < 0.05$, 0.01 or 0.001, respectively. $^{+}$, $^{++}$ or $^{+++}$ indicates values significantly different from the low dose of FSD 8 at $P < 0.05$, 0.01 or 0.001, respectively.

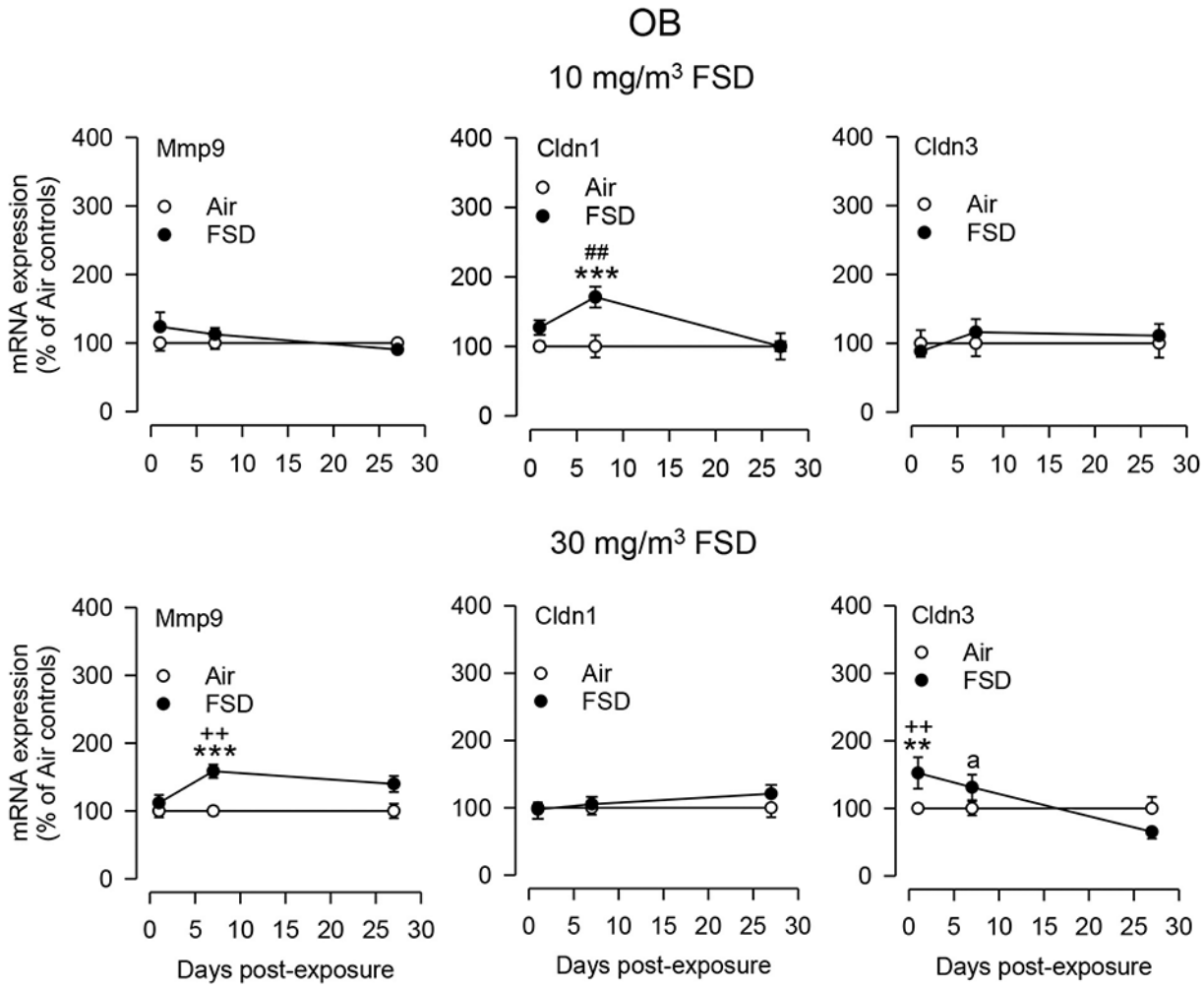

Fig. 7.

mRNA expression of blood-brain barrier associated markers in the olfactory bulb (OB). Rats were exposed to FSD 8 aerosol (10 or 30 mg/m^3; 6 h/d × 4 d) by whole-body inhalation. At 1, 7 or 27 d post-exposure, the mRNA expression of *Mmp9, Cldn1* and *Cldn3* were assayed by TaqMan real-time PCR. Following normalization to the endogenous control β-actin (*Actb*), the change in mRNA expression was calculated as percent of air-exposed controls. n = 6/group. $^*P < 0.05$, $^{**}P < 0.01$, $^{***}P < 0.001$. $^{\#}$, $^{\#\#}$ or $^{\#\#\#}$ indicates values significantly different from the high dose FSD 8 at $P < 0.05$, 0.01 or 0.001, respectively. $^{+}$, $^{++}$ or $^{+++}$ indicates values significantly different from the low dose of FSD 8 at $P < 0.05$, 0.01 or 0.001, respectively.

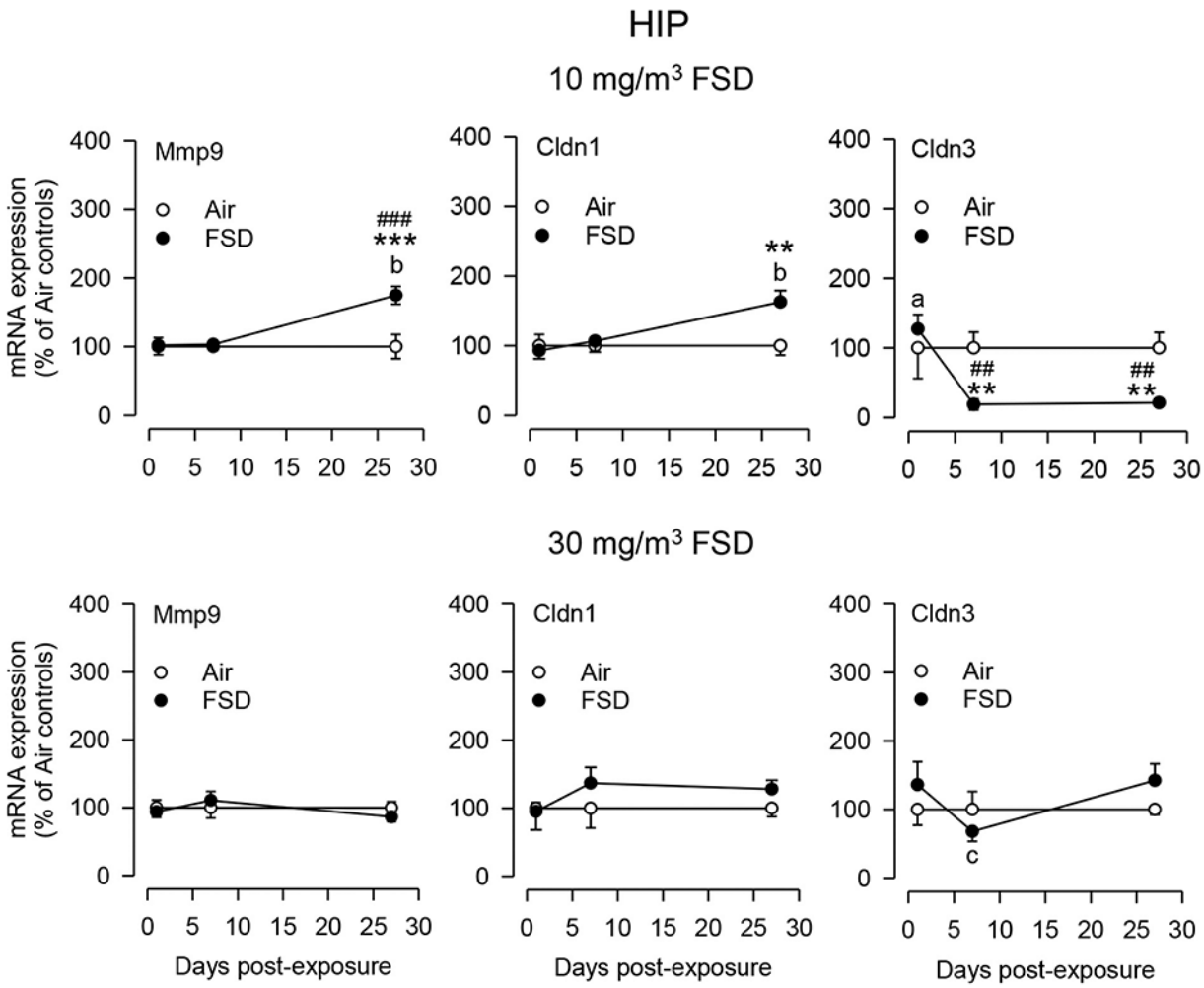

Fig. 8.

mRNA expression of blood-brain barrier associated markers in the hippocampus (HIP). Rats were exposed to FSD 8 aerosol (10 or 30 mg/m^3; 6 h/d × 4 d) by whole-body inhalation. At 1, 7 or 27 d post-exposure, the mRNA expression of *Mmp9, Cldn1* and *Cldn3* were assayed by TaqMan real-time PCR. Following normalization to the endogenous control β-actin (*Actb*), the change in mRNA expression was calculated as percent of air-exposed controls. n = 4–6/group. $^b n = 4$ due to two outlier sample in assay group; $^*P < 0.05$, $^{**}P < 0.01$, $^{***}P < 0.001$. $^{\#}$, $^{\#\#}$ or $^{\#\#\#}$ indicates values significantly different from the low dose of FSD 8 at $P <$ 0.05, 0.01 or 0.001, respectively. $^{+}$, $^{++}$ or $^{+++}$ indicates values significantly different from low dose FSD 8 at $P < 0.05$, 0.01 or 0.001, respectively.

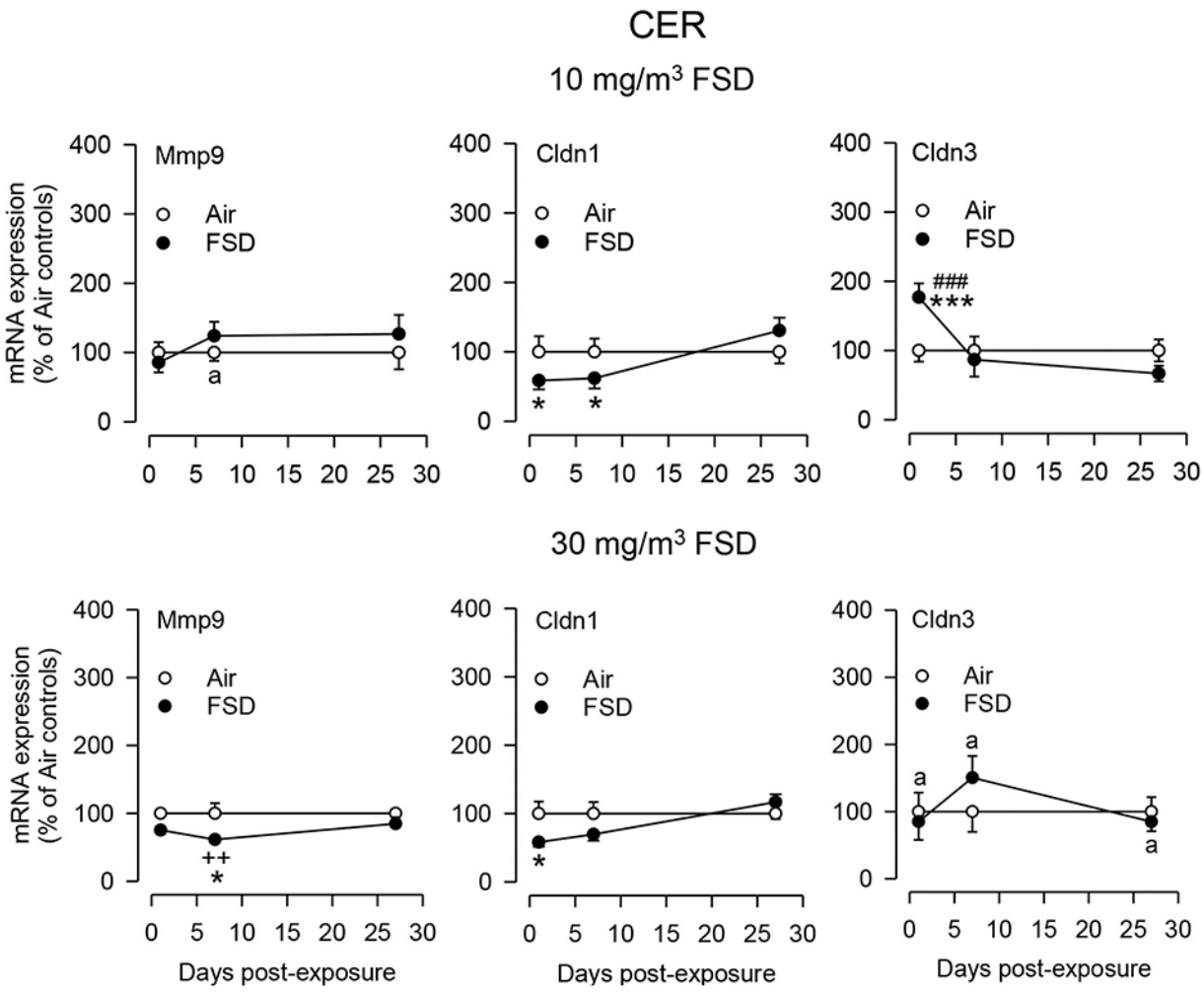

Fig. 9.

mRNA expression of blood-brain barrier associated markers in the cerebellum (CER). Rats were exposed to FSD 8 aerosol (10 or 30 mg/m^3; 6 h/d × 4 d) by whole-body inhalation. At 1, 7 or 27 d post-exposure, the mRNA expression of *Mmp9, Cldn1* and *Cldn3* were assayed by TaqMan real-time PCR. Following normalization to the endogenous control β-actin (*Actb*), the change in mRNA expression was calculated as percent of air-exposed controls. n = 5-6/group. $^a n = 5$ due to one outlier sample in assay group; $^*P < 0.05$, $^{**}P < 0.01$, $^{***}P < 0.001$. $^{\#}$, $^{\#\#}$ or $^{\#\#\#}$ indicates values significantly different from the high dose FSD 8 at $P <$ 0.05, 0.01 or 0.001, respectively. $^{+}$, $^{++}$ or $^{+++}$ indicates values significantly different from the low dose of FSD 8 at $P < 0.05$, 0.01 or 0.001, respectively.

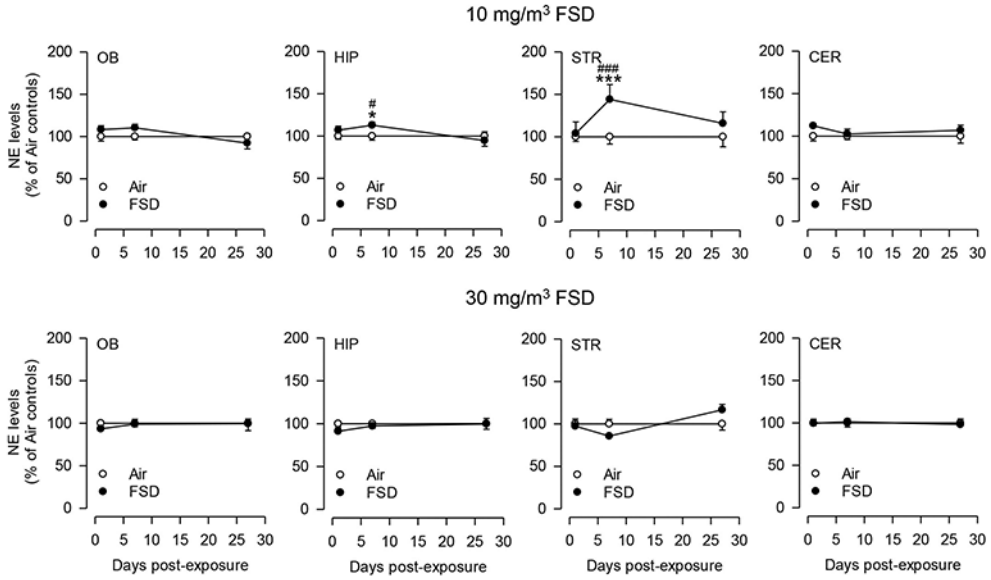

Fig. 10.

Changes in the levels of norepinephrine in various brain regions. Rats were exposed to FSD 8 aerosol (10 or 30 mg/m^3; 6 h/d × 4 d) by whole-body inhalation. At 1, 7 or 27 d post-exposure, the levels of norepinephrine (NE) were measured by HPLC-EC in the olfactory bulb (OB), hippocampus (HIP), striatum (STR) and cerebellum (CER). Following normalization to an internal standard, the neurotransmitter content was calculated using a standard curve. Values are expressed as percent of air-exposed controls. n = 7–8/group). *P < 0.05, **P < 0.01, ***P < 0.001. $^{\#}$, $^{\#\#}$ or $^{\#\#\#}$ indicates values significantly different from the high dose FSD 8 at P < 0.05, 0.01 or 0.001, respectively. $^{+}$, $^{++}$ or $^{+++}$ indicates values significantly different from the low dose of FSD 8 at P < 0.05, 0.01 or 0.001, respectively.

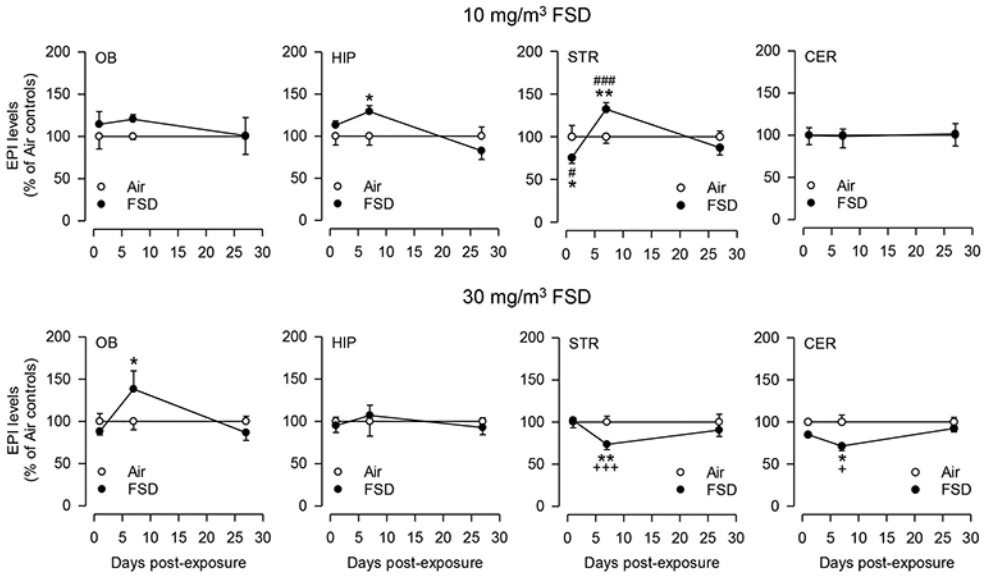

Fig. 11.

Changes in the levels of epinephrine in various brain regions. Rats were exposed to FSD 8 aerosol (10 or 30 mg/m^3; 6 h/d × 4 d) by whole-body inhalation. At 1, 7 or 27 d post-exposure, the levels of epinephrine (EPI) were measured by HPLC-EC in the olfactory bulb (OB), hippocampus (HIP), striatum (STR) and cerebellum (CER). Following normalization to an internal standard, the neurotransmitter content was calculated using a standard curve. Values are expressed as percent of air-exposed controls. n = 8/group. *P < 0.05, **P < 0.01, ***P < 0.001. $^{\#}$, $^{\#\#}$ or $^{\#\#\#}$ indicates values significantly different from the high dose FSD 8 at P < 0.05, 0.01 or 0.001, respectively. $^{+}$, $^{++}$ or $^{+++}$ indicates values significantly different from the low dose of FSD 8 at P < 0.05, 0.01 or 0.001, respectively.

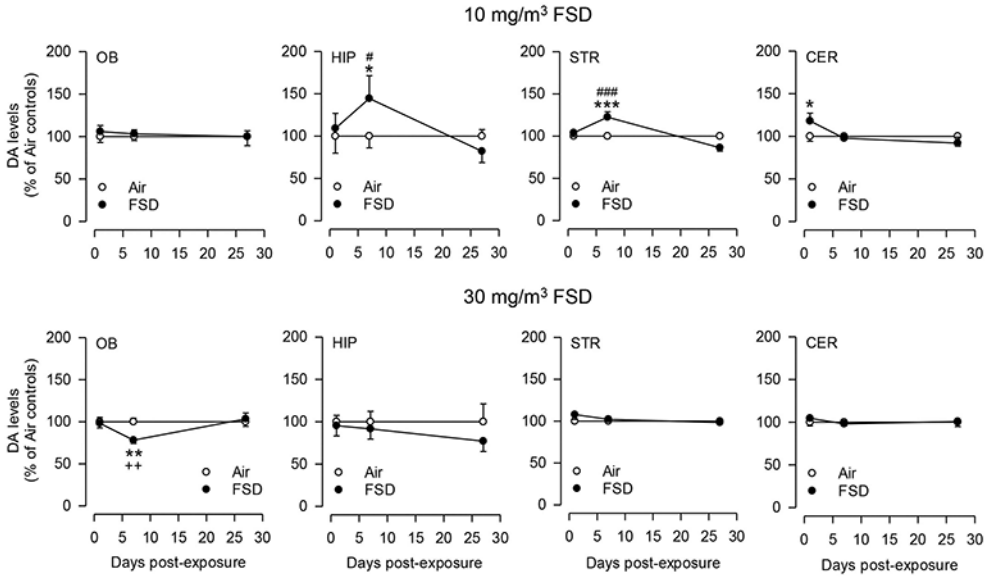

Fig. 12.

Changes in the levels of dopamine in various brain regions. Rats were exposed to FSD 8 aerosol (10 or 30 mg/m^3; 6 h/d × 4 d) by whole-body inhalation. At 1, 7 or 27 d post-exposure, the levels of dopamine (DA) were measured by HPLC-EC in the olfactory bulb (OB), hippocampus (HIP), striatum (STR) and cerebellum (CER). Following normalization to an internal standard, the neurotransmitter content was calculated using a standard curve. Values are expressed as percent of air-exposed controls. n = 8/group. *P < 0.05, **P < 0.01, ***P < 0.001. $^{\#}$, $^{\#\#}$ or $^{\#\#\#}$ indicates values significantly different from the high dose FSD 8 at P < 0.05, 0.01 or 0.001, respectively. $^{+}$, $^{++}$ or $^{+++}$ indicates values significantly different from the low dose of FSD 8 at P < 0.05, 0.01 or 0.001, respectively.

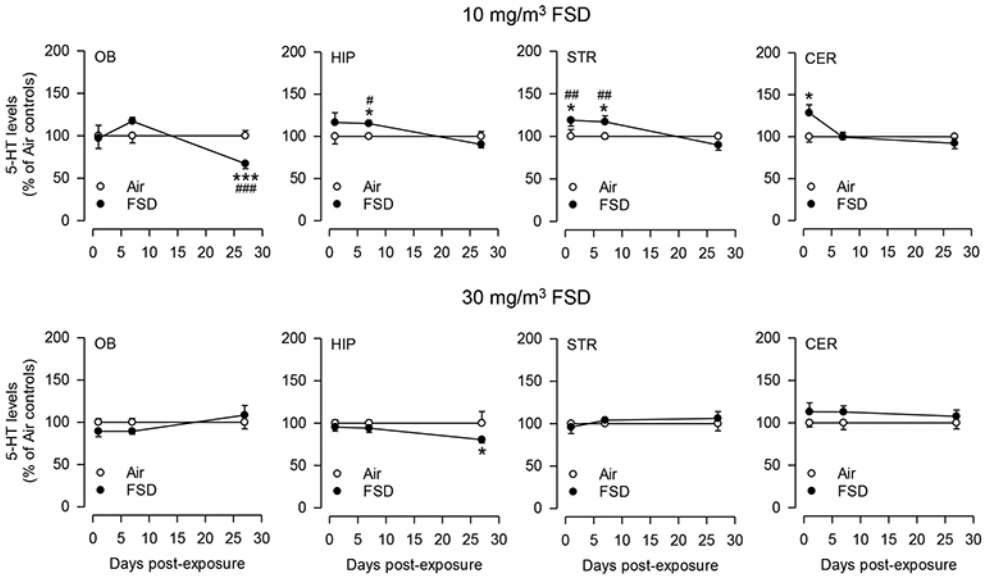

Fig. 13.

Changes in the levels of serotonin in various brain regions. Rats were exposed to FSD 8 aerosol (10 or 30 mg/m^3; 6 h/d × 4 d) by whole-body inhalation. At 1, 7 or 27 d post-exposure, the levels of serotonin (5-HT) were measured by HPLC-EC in the olfactory bulb (OB), hippocampus (HIP), striatum (STR) and cerebellum (CER). Following normalization to an internal standard, the neurotransmitter content was calculated using a standard curve. Values are expressed as percent of air-exposed controls. n = 7–8/group. *P < 0.05, **P < 0.01, ***P < 0.001. $^{\#}$, $^{\#\#}$ or $^{\#\#\#}$ indicates values significantly different from the high dose FSD 8 at P < 0.05, 0.01 or 0.001, respectively. $^{+}$, $^{++}$ or $^{+++}$ indicates values significantly different from the low dose of FSD 8 at P < 0.05, 0.01 or 0.001, respectively.

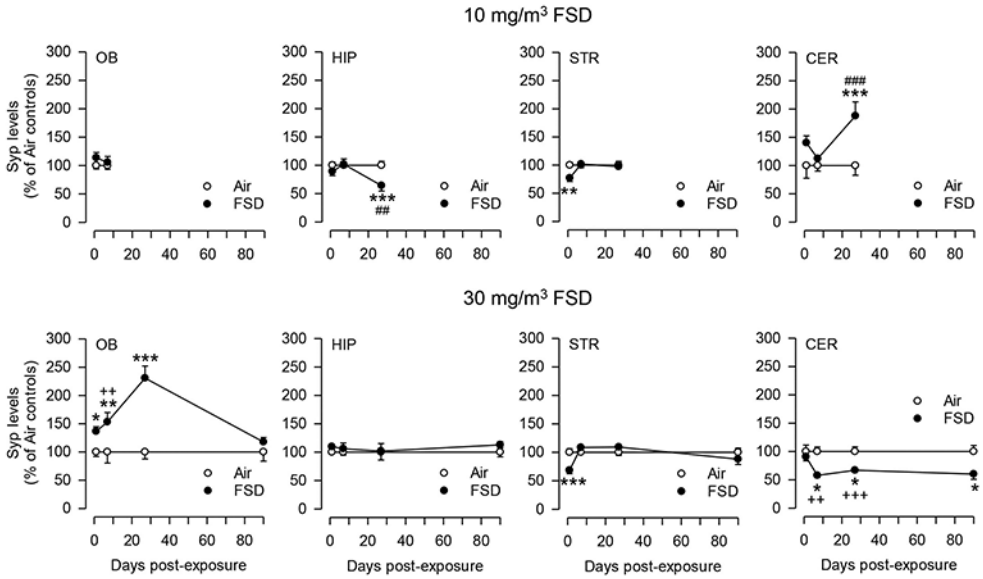

Fig. 14.

Levels of synaptophysin-1 protein in various brain regions. Rats were exposed to FSD 8 aerosol (10 or 30 mg/m^3; 6 h/d × 4 d) by whole-body inhalation. At 1, 7, 27 or 90 d post-exposure, the protein expression of synaptophysin-1 (SYP) was determined by western immunoblotting in the olfactory bulb (OB), hippocampus (HIP), striatum (STR) and cerebellum (CER). Following normalization to the endogenous control β-actin (ACTB), the change in protein expression was calculated as percent of air-exposed controls. Values are expressed as percent of air-exposed controls. n = 7–8/group. *P < 0.05, **P < 0.01, ***P < 0.001. $^{\#}$, $^{\#\#}$ or $^{\#\#\#}$ indicates values significantly different from the high dose FSD 8 at P < 0.05, 0.01 or 0.001, respectively. $^{+}$, $^{++}$ or $^{+++}$ indicates values significantly different from the low dose of FSD 8 at P < 0.05, 0.01 or 0.001, respectively. OB tissue from the 27-d time point of the low dose FSD 8 exposure was not collected.

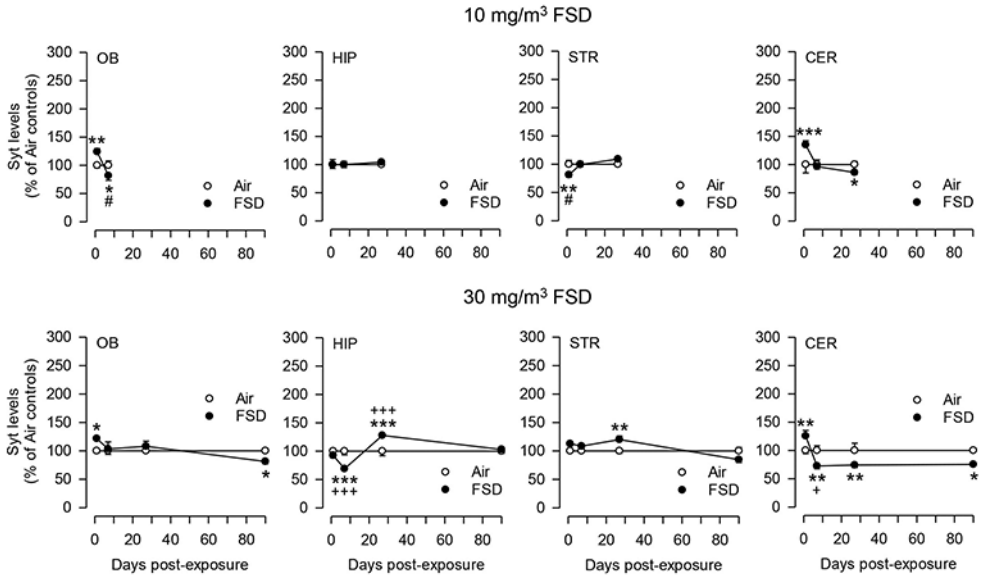

Fig. 15.

Levels of synaptotagmin-1 protein in various brain regions. Rats were exposed to FSD 8 aerosol (10 or 30 mg/m^3; 6 h/d × 4 d) by whole-body inhalation. At 1, 7, 27 or 90 d post-exposure, the protein expression of synaptotagmin-1 (SYT) was determined by western immunoblotting in the olfactory bulb (OB), hippocampus (HIP), striatum (STR) and cerebellum (CER). Following normalization to the endogenous control β-actin (ACTB), the change in protein expression was calculated as percent of air-exposed controls. Values are expressed as percent of air-exposed controls. n = 7–8/group. *P < 0.05, **P < 0.01, ***P < 0.001. $^{\#}$, $^{\#\#}$ or $^{\#\#\#}$ indicates values significantly different from the high dose FSD 8 at P < 0.05, 0.01 or 0.001, respectively. $^{+}$, $^{++}$ or $^{+++}$ indicates values significantly different from the low dose of FSD 8 at P < 0.05, 0.01 or 0.001, respectively. OB tissue from the 27-d time point of the low dose FSD 8 exposure was not collected.

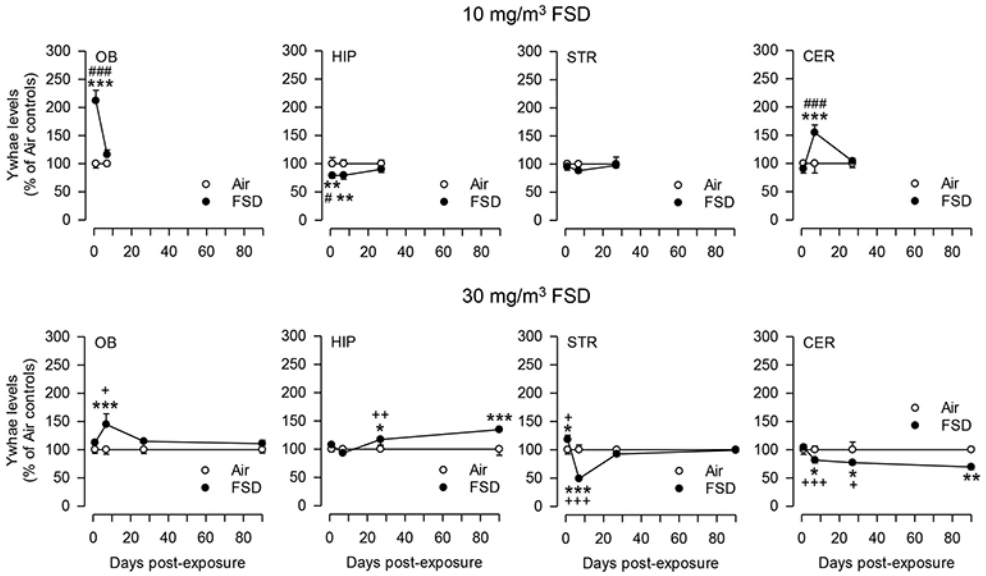

Fig. 16.

Levels of tyrosine 3-monooxygenase/tryptophan 5-monooxygenase activation protein-ε–protein in various brain regions. Rats were exposed to FSD 8 aerosol (10 or 30 mg/m^3; 6 h/d × 4 d) by whole-body inhalation. At 1, 7, 27 or 90 d post-exposure, the protein expression of tyrosine 3-monooxygenase/tryptophan 5-monooxygenase activation protein-14-3-3-ε (YWHAE) was determined by western immunoblotting in the olfactory bulb (OB), hippocampus (HIP), striatum (STR) and cerebellum (CER). Following normalization to the endogenous control β-actin (ACTB), the change in protein expression was calculated as percent of air-exposed controls. Values are expressed as percent of air-exposed controls. n = 7–8/group. *$P < 0.05$, **$P < 0.01$, ***$P < 0.001$. $^{\#}$, $^{\#\#}$ or $^{\#\#\#}$ indicates values significantly different from the high dose FSD 8 at $P < 0.05$, 0.01 or 0.001, respectively. $^{+}$, $^{++}$ or $^{+++}$ indicates values significantly different from the low dose of FSD 8 at $P < 0.05$, 0.01 or 0.001, respectively. OB tissue from the 27-d time point of the low dose FSD 8 exposure was not collected.

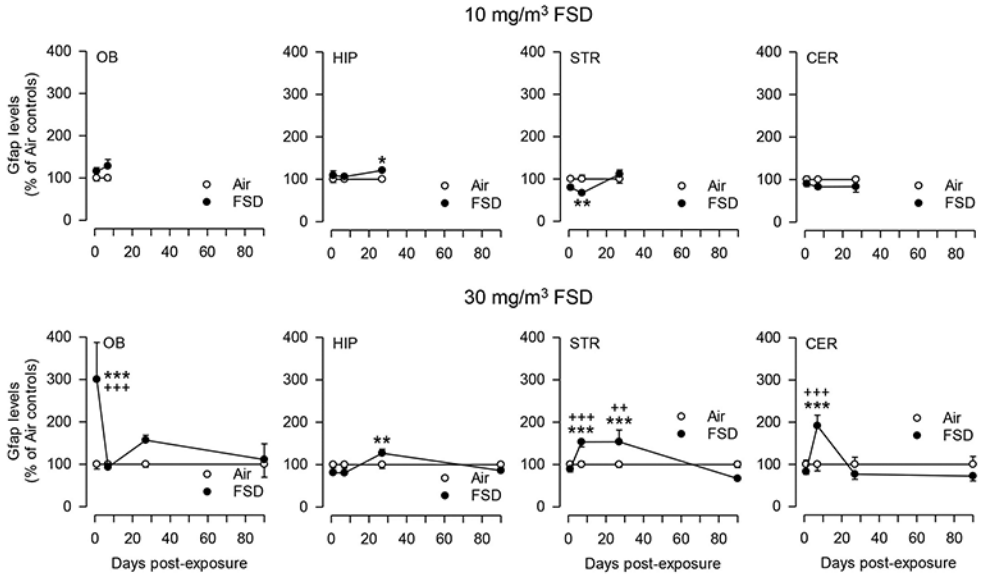

Fig. 17.

Levels of glial fibrillary acidic protein in various brain regions. Rats were exposed to FSD 8 aerosol (10 or 30 mg/m^3; 6 h/d × 4 d) by whole-body inhalation. At 1, 7, 27 or 90 d post-exposure, the protein expression of glial fibrillary acidic protein (GFAP) was determined by western immunoblotting in the olfactory bulb (OB), hippocampus (HIP), striatum (STR) and cerebellum (CER). Following normalization to the endogenous control β-actin (ACTB), the change in protein expression was calculated as percent of air-exposed controls. Values are expressed as percent of air-exposed controls. n = 6–8/group. *P < 0.05, **P < 0.01, ***P < 0.001. $^{\#}$, $^{\#\#}$ or $^{\#\#\#}$ indicates values significantly different from the high dose FSD 8 at P < 0.05, 0.01 or 0.001, respectively. $^{+}$, $^{++}$ or $^{+++}$ indicates values significantly different from the low dose of FSD 8 at P < 0.05, 0.01 or 0.001, respectively. OB tissue from the 27-d time point of the low dose FSD 8 exposure was not collected.

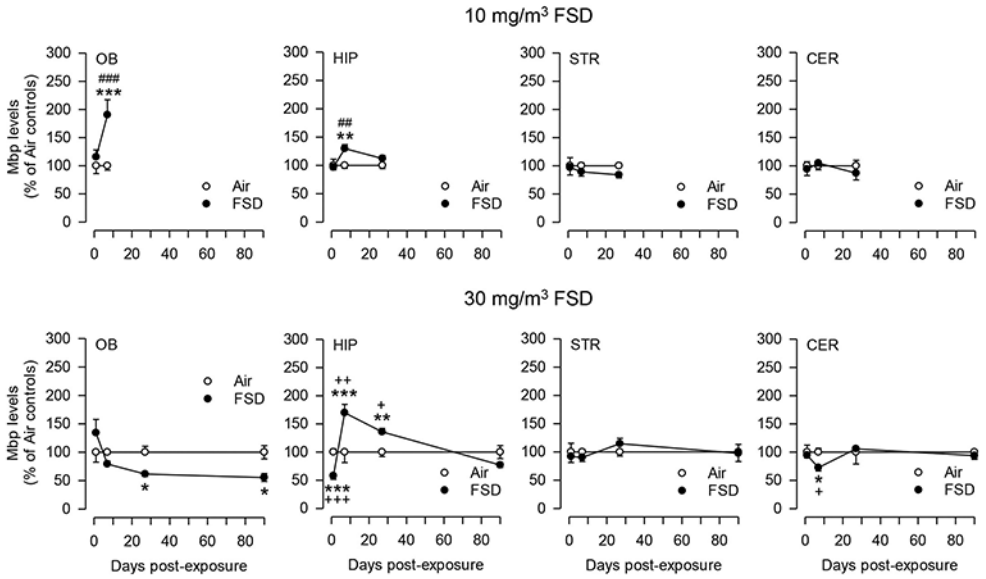

Fig. 18.

Levels of myelin basic protein in various brain regions. Rats were exposed to FSD 8 aerosol (10 or 30 mg/m^3; 6 h/d × 4 d) by whole-body inhalation. At 1, 7, 27 or 90 d post-exposure, the protein expression of myelin basic protein (MBP) was determined by western immunoblotting in the olfactory bulb (OB), hippocampus (HIP), striatum (STR) and cerebellum (CER). Following normalization to the endogenous control β-actin (ACTB), the change in protein expression was calculated as percent of air-exposed controls. Values are expressed as percent of air-exposed controls. n = 6–8/group. *P < 0.05, **P < 0.01, ***P < 0.001. $^{\#}$, $^{\#\#}$ or $^{\#\#\#}$ indicates values significantly different from the high dose FSD 8 at P < 0.05, 0.01 or 0.001, respectively. $^{+}$, $^{++}$ or $^{+++}$ indicates values significantly different from the low dose of FSD 8 at P < 0.05, 0.01 or 0.001, respectively. OB tissue from the 27-d time point of the low dose FSD 8 exposure was not collected.

Table 1

Metabolites of dopamine and serotonin in olfactory bulb and hippocampus.

Brain Region	Group	Dose	DOPAC	HVA	5-HIAA
OB	Air (1 d)	0	100.0 ± 6.3	100.0 ± 7.6	100.0 ± 14.7
	FSD 8 (1 d)	10 mg/m^3	107.3 ± 7.1	104.2 ± 3.8	99.4 ± 16.6
	Air (7 d)	0	100.0 ± 6.2	100.0 ± 4.5	100.0 ± 11.1
	FSD 8 (7 d)	10 mg/m^3	99.2 ± 6.6	97.5 ± 3.8	92.2 ± 5.6
	Air (27 d)	0	100.0 ± 4.6	100.0 ± 11.9	100.0 ± 7.2
	FSD 8 (27 d)	10 mg/m^3	84.2 ± 7.8	90.6 ± 13.2	92.2 ± 5.1
	Air (1 d)	0	100.0 ± 7.5	100.0 ± 7.4	100.0 ± 15.0
	FSD 8 (1 d)	30 mg/m^3	101.3 ± 4.2	89.9 ± 3.5	76.8 ± 9.5
	Air (7 d)	0	100.0 ± 3.7	100.0 ± 5.7	100.0 ± 4.8
	FSD 8 (7 d)	30 mg/m^3	78.1 ± 4.6*	79.0 ± 3.3*	82.5 ± 4.4
	Air (27 d)	0	100.0 ± 4.1	100.0 ± 5.2	100.0 ± 8.5
	FSD 8 (27 d)	30 mg/m^3	94.3 ± 4.0	85.7 ± 5.4	108.3 ± 8.6
HIP	Air (1 d)	0	100.0 ± 6.8	100.0 ± 9.3	100.0 ± 8.3
	FSD 8 (1 d)	10 mg/m^3	107.5 ± 10.0	98.5 ± 7.4^d	100.9 ± 12.5
	Air (7 d)	0	100.0 ± 5.7	100.0 ± 5.9	100.0 ± 7.8
	FSD 8 (7 d)	10 mg/m^3	121.4 ± 8.3	137.2 ± 12.4$^\#$	114.3 ± 3.7
	Air (27 d)	0	100.0 ± 8.3	100.0 ± 4.3	100.0 ± 3.1
	FSD 8 (27 d)	10 mg/m^3	84.6 ± 5.5	72.4 ± 6.4	84.6 ± 4.2
	Air (1 d)	0	100.0 ± 3.9	100.0 ± 14.2	100.0 ± 4.4
	FSD 8 (1 d)	30 mg/m^3	102.7 ± 3.7	83.5 ± 7.4	92.8 ± 3.5
	Air (7 d)	0	100.0 ± 5.1	100.0 ± 11.4	100.0 ± 4.6
	FSD 8 (7 d)	30 mg/m^3	86.9 ± 3.4	83.8 ± 6.3	80.2 ± 8.4
	Air (27 d)	0	100.0 ± 16.3	100.0 ± 8.3	100.0 ± 6.0
	FSD 8 (27 d)	30 mg/m^3	95.2 ± 5.1	78.9 ± 4.0^c	93.7 ± 4.2

Values were calculated as ng/mg protein and are expressed as percent of corresponding air-exposed control. Data are mean SE (n = 8/group with the following exceptions

^{c} n = 7 due to one undetected sample in assay group

^{d} n = 6 due to two undetected samples in assay group).

* Significant decrease from corresponding air-exposed control ($P < 0.05$).

$^\#$ Significant increase from corresponding air-exposed control ($P < 0.05$).

Table 2

Metabolites of dopamine and serotonin in striatum and cerebellum.

Brain Region	Group	Dose	DOPAC	HVA	5-HIAA
STR	Air (1 d)	0	100.0 ± 9.3	100.0 ± 6.2	100.0 ± 8.8
	FSD 8 (1 d)	10 mg/m^3	93.9 ± 6.2	97.6 ± 3.6	102.8 ± 5.0
	Air (7 d)	0	100.0 ± 4.8	100.0 ± 3.6	100.0 ± 8.0
	FSD 8 (7 d)	10 mg/m^3	121.1 ± 5.0	118.1 ± 5.9	97.6 ± 4.5
	Air (27 d)	0	100.0 ± 6.1	100.0 ± 7.5	100.0 ± 3.6
	FSD 8 (27 d)	10 mg/m^3	78.4 ± 4.6*	82.2 ± 6.5	82.3 ± 4.3
	Air (1 d)	0	100.0 ± 3.0	100.0 ± 4.8	100.0 ± 4.3
	FSD 8 (1 d)	30 mg/m^3	109.6 ± 6.4	104.9 ± 6.1	94.9 ± 6.5
	Air (7 d)	0	100.0 ± 5.9	100.0 ± 4.7	100.0 ± 4.5
	FSD 8 (7 d)	30 mg/m^3	92.4 ± 3.1	92.1 ± 3.9	97.6 ± 4.9
	Air (27 d)	0	100.0 ± 2.3	100.0 ± 3.6	100.0 ± 6.9
	FSD 8 (27 d)	30 mg/m^3	97.2 ± 5.1	89.1 ± 6.2	101.8 ± 6.8
CER	Air (1 d)	0	100.0 ± 4.0	100.0 ± 5.4	100.0 ± 5.6
	FSD 8 (1 d)	10 mg/m^3	109.5 ± 4.8	100.2 ± 5.7	111.8 ± 4.7
	Air (7 d)	0	100.0 ± 4.4	100.0 ± 5.7	100.0 ± 3.4
	FSD 8 (7 d)	10 mg/m^3	104.9 ± 2.6	103.6 ± 3.2	106.5 ± 3.2
	Air (27 d)	0	100.0 ± 8.3	100.0 ± 9.7	100.0 ± 9.0
	FSD 8 (27 d)	10 mg/m^3	97.0 ± 5.0	109.2 ± 7.5	96.9 ± 4.7
	Air (1 d)	0	100.0 ± 6.5	100.0 ± 6.5	100.0 ± 4.8
	FSD 8 (1 d)	30 mg/m^3	102.3 ± 5.0	88.9 ± 3.6	97.8 ± 4.5
	Air (7 d)	0	100.0 ± 3.8	100.0 ± 4.4	100.0 ± 3.0
	FSD 8 (7 d)	30 mg/m^3	88.4 ± 5.2[a]	92.8 ± 3.9	107.4 ± 4.6
	Air (27 d)	0	100.0 ± 9.3	100.0 ± 6.2	100.0 ± 4.8
	FSD 8 (27 d)	30 mg/m^3	102.4 ± 4.3	92.1 ± 12.6	94.9 ± 6.3

Values were calculated as ng/mg protein and are expressed as percent of corresponding air-exposed control. Data are mean ± SE (n = 8/group with the following exception:

[a] $n = 7$ due to one outlier sample in assay group).

* Significant decrease from corresponding air-exposed control ($P < 0.05$).

Table 3

Dopamine and serotonin metabolite ratios in the olfactory bulb and hippocampus.

Brain Region	Group	Dose	DOPAC/DA	HVA/DA	(DOPAC + HVA)/DA	5-HIAA/5-HT
OB	Air (1 d)	0	100 ± 3.9	100 ± 4.2	100 ± 4.0	100 ± 12.6
	FSD 8 (1 d)	10 mg/m^3	103.1 ± 3.9	99.7 ± 3.9	100.3 ± 3.9	102.1 ± 3.9
	Air (7 d)	0	100 ± 5.4	100 ± 4.9	100 ± 4.7	100 ± 5.3
	FSD 8 (7 d)	10 mg/m^3	96.6 ± 3.1	96.2 ± 3.1	96.2 ± 2.8	80.8 ± 5.8
	Air (27 d)	0	100 ± 5.7	100 ± 7.1	100 ± 4.8	100 ± 8.6
	FSD 8 (27 d)	10 mg/m^3	84.0 ± 4.5 *	91.0 ± 7.9	88.0 ± 6.0	138.3 ± 7.7 $^{\#}$
	Air (1 d)	0	100 ± 6.2	100 ± 3.8	100 ± 4.2	100 ± 12.4
	FSD 8 (1 d)	30 mg/m^3	105.6 ± 7.9	93.4 ± 4.8	98.2 ± 6.0	88.3 ± 11.0
	Air (7 d)	0	100 ± 6.4	100 ± 3.7	100 ± 3.6	100 ± 3.6
	FSD 8 (7 d)	30 mg/m^3	98.7 ± 3.6	102.1 ± 5.0	100.8 ± 3.2	92.2 ± 4.1
	Air (27 d)	0	100 ± 4.0	100 ± 4.5	100 ± 3.7	100 ± 7.3
	FSD 8 (27 d)	30 mg/m^3	91.9 ± 4.2	83.2 ± 4.6	87.0 ± 4.0	102.7 ± 9.4
HIP	Air (1 d)	0	100 ± 14.3	100 ± 12.6	100 ± 13.7	100 ± 3.5
	FSD 8 (1 d)	10 mg/m^3	88.1 ± 7.9	83.9 ± 10.2 ^{d}	81.9 ± 8.8	85.0 ± 6.5
	Air (7 d)	0	100 ± 17.3	100 ± 13.9	100 ± 15.0	100 ± 2.9
	FSD 8 (7 d)	10 mg/m^3	83.9 ± 14.6 ^{c}	91.3 ± 12.1 $^{(c)}$	87.6 ± 12.8 ^{c}	97.9 ± 2.0 ^{c}
	Air (27 d)	0	100 ± 8.7	100 ± 6.2	100 ± 6.7	100 ± 4.5
	FSD 8 (27 d)	10 mg/m^3	127.3 ± 27.2	104.1 ± 16.6	119.3 ± 23.3	93.1 ± 5.4
	Air (1 d)	0	100 ± 8.6	100 ± 9.3	100 ± 7.2	100 ± 3.0
	FSD 8 (1 d)	30 mg/m^3	114.1 ± 13.0	94.4 ± 7.6	111.9 ± 12.3	97.7 ± 2.3
	Air (7 d)	0	100 ± 9.0	100 ± 9.3	100 ± 8.4	100 ± 4.0
	FSD 8 (7 d)	30 mg/m^3	100.1 ± 13.8	99.2 ± 13.7	100 ± 13.6	83.5 ± 7.7
	Air (27 d)	0	100 ± 23.3	100 ± 12.5	100 ± 19.0	100 ± 9.3
	FSD 8 (27 d)	30 mg/m^3	108.9 ± 12.5	87.9 ± 10.0 ^{c}	101.6 ± 12 ^{c}	108.1 ± 5.0

Values were calculated as ng/mg protein. The ratios DOPAC/DA, HVA/DA, (DOPAC+HVA)/DA, and 5-HIAA/5-HT were determined and are expressed as percent of corresponding air-exposed control. Data are mean ± SE (n = 8/group with the following exceptions:

^{c} n = 7 due to one undetected sample in assay group

[d] $n = 6$ due to two undetected samples in assay group).

[*] Significant decrease from corresponding air-exposed control ($P < 0.05$).

[#] Significant increase from corresponding air-exposed control ($P < 0.05$).

Table 4

Dopamine and serotonin metabolite ratios in the striatum and cerebellum.

Brain Region	Group	Dose	DOPAC/DA	HVA/DA	(DOPAC + HVA)/DA	5-HIAA/5-HT
STR	Air (1 d)	0	100 ± 5.4	100 ± 4.3	100 ± 4.4	100 ± 3.0
	FSD 8 (1 d)	10 mg/m^3	91.0 ± 2.9	94.1 ± 2.7	92.6 ± 2.1	87.2 ± 3.4
	Air (7 d)	0	100 ± 4.8	100 ± 3.3	100 ± 3.8	100 ± 8.2
	FSD 8 (7 d)	10 mg/m^3	99.2 ± 3.2	96.9 ± 4.5	97.9 ± 3.5	83.7 ± 3.0
	Air (27 d)	0	100 ± 4.8	100 ± 5.4	100 ± 4.7	100 ± 3.7
	FSD 8 (27 d)	10 mg/m^3	91.5 ± 4.4	96.3 ± 7.0	93.6 ± 5.0	96.0 ± 3.9
	Air (1 d)	0	100 ± 2.3	100 ± 3.2	100 ± 2.3	100 ± 3.4
	FSD 8 (1 d)	30 mg/m^3	101.5 ± 1.6	97.4 ± 1.2	99.9 ± 1.0	99.9 ± 2.7
	Air (7 d)	0	100 ± 2.7	100 ± 4.6	100 ± 3.0	100 ± 3.7
	FSD 8 (7 d)	30 mg/m^3	90.3 ± 1.3	89.0 ± 2.0	89.7 ± 1.3	92.7 ± 3.3
	Air (27 d)	0	100 ± 3.8	100 ± 5.0	100 ± 4.1	100 ± 3.5
	FSD 8 (27 d)	30 mg/m^3	98.6 ± 5.1	89.9 ± 5.2	95.1 ± 4.8	96.4 ± 5.7
CER	Air (1 d)	0	100 ± 4.1	100 ± 3.9	100 ± 3.5	100 ± 3.4
	FSD 8 (1 d)	10 mg/m^3	95.0 ± 7.8	87.9 ± 8.2	91.5 ± 7.6	90.0 ± 7.8
	Air (7 d)	0	100 ± 5.2	100 ± 6.2	100 ± 5.0	100 ± 4.0
	FSD 8 (7 d)	10 mg/m^3	108.4 ± 6.2	106.3 ± 4.1	107.3 ± 4.7	108.6 ± 6.2
	Air (27 d)	0	100 ± 12.3	100 ± 13.3	100 ± 10.3	100 ± 9.6
	FSD 8 (27 d)	10 mg/m^3	100.4 ± 6.5	112.7 ± 10.5	105.2 ± 6.5	99.4 ± 5.5
	Air (1 d)	0	100 ± 5.0	100 ± 3.7	100 ± 4.3	100 ± 4.3
	FSD 8 (1 d)	30 mg/m^3	100.8 ± 8.7	87.0 ± 4.8	98.6 ± 7.9	90.2 ± 7.8
	Air (7 d)	0	100 ± 6.6 [a]	100 ± 4.8[a]	100 ± 5.7[a]	100 ± 5.8
	FSD 8 (7 d)	30 mg/m^3	89.5 ± 6.9	94.5 ± 5.4	90.3 ± 6.2	94.1 ± 5.6
	Air (27 d)	0	100 ± 11.3	100 ± 7.4	100 ± 10.5	100 ± 6.2
	FSD 8 (27 d)	30 mg/m^3	99.5 ± 4.4	88.9 ± 9.9	98.5 ± 4.5	88.3 ± 6.8

Values were calculated as ng/mg protein. The ratios DOPAC/DA, HVA/DA, (DOPAC+HVA)/DA, and 5-HIAA/5-HT were determined and are expressed as percent of corresponding air-exposed control. Data are mean ± SE (n = 8/group with the following exception:

[a] n = 7 due to one outlier sample in assay group).